GEODYNAMICS & TECTONOPHYSICS

PUBLISHED BY THE INSTITUTE OF THE EARTH'S CRUST
SIBERIAN BRANCH OF RUSSIAN ACADEMY OF SCIENCES

2018 VOLUME 9 ISSUE 3 PAGES 855–888 ISSN 2078-502X

https://doi.org/10.5800/GT-2018-9-3-0374

GEODYNAMIC CONDITIONS FOR CENOZOIC ACTIVATION OF TECTONIC STRUCTURES IN SOUTHEASTERN MONGOLIA

A. V. Parfeevets[1], V. A. Sankov[1, 2]

[1] *Institute of the Earth's Crust, Siberian Branch of RAS, Irkutsk, Russia*
[2] *Irkutsk State University, Irkutsk, Russia*

Abstract: The knowledge of the neotectonic structures in Southeastern Mongolia, that is considerably distant from the active plate boundaries, is important for determining a source of tectonic deformation and regular features of activation in the intracontinental setting. Our research was focused on the East Gobi and South Gobi depressions located in Southeastern Mongolia, which developed since the Mesozoic and were activated to various degrees in the neotectonic stage. The study aimed to assess the paleostress state of the crust in Southeastern Mongolia, identify the stages, factors and mechanisms of the Cenozoic activation of the regional structures of different strike, and determine the sources of activation. The analysis of the available literature suggests a similar history of their development in the Late Jurassic – Early Cretaceous (rifting) and Late Cretaceous – Paleogene (tectonic quiescence). In the Cenozoic stage, the depressions experienced activation of completely different styles. In the East Gobi depression, left-lateral strike-slip faults were activated in the Tertiary, and the post-Late Cretaceous thrusting took place along the northeastern faults on the northern slope of the Totoshan uplift. In the Early Cenozoic, the N-S and N-W compression was dominant as evidenced by the deformed Late Cretaceous sediments and the reconstructed stress tensors typical of the compression and transpression regimes. An overview of the published data suggests that the most probable cause of such deformation was the impact of the Western Pacific zone of plate interaction. However, a potential influence of compression at the early stages of the Indo-Asian collision cannot be completely excluded. The East Gobi depression was low active in the second half of the Cenozoic. In contrast to the East Gobi depression, the South Gobi activation began in the Late Cenozoic (Late Miocene – Early Pliocene). Young uplifts and forbergs (Gobi Altai eastern termination) developed actively and 'cut' the sediments of the basins originating from the Mesozoic. The W-E and N-W strike-slip and thrust faults were active in the Pliocene–Quaternary. The stress field reconstructions show compression, transpression and strike-slip regimes with the NE-trending axis of compression. Deformation in the East Goby Altay (as well as in Western and Southwestern Mongolia) is driven by the India-Eurasia collision.

Key words: Cenozoic; neotectonic structure; paleostress; active fault; Southeastern Mongolia

RESEARCH ARTICLE

Handling Editor: S.A. Bornyakov

Received: June 8, 2018
Revised: July 4, 2018
Accepted: August 2, 2018

For citation: *Parfeevets A.V., Sankov V.A.*, 2018. Geodynamic conditions for Cenozoic activation of tectonic structures in Southeastern Mongolia. *Geodynamics & Tectonophysics* 9 (3), 855–888. doi:10.5800/GT-2018-9-3-0374.

ГЕОДИНАМИЧЕСКИЕ УСЛОВИЯ КАЙНОЗОЙСКОЙ АКТИВИЗАЦИИ ТЕКТОНИЧЕСКИХ СТРУКТУР ЮГО-ВОСТОЧНОЙ МОНГОЛИИ

А. В. Парфеевец[1], В. А. Саньков[1, 2]

[1] *Институт земной коры СО РАН, Иркутск, Россия*
[2] *Иркутский государственный университет, Иркутск, Россия*

Аннотация: Неотектонические структуры юго-восточной части территории Монголии значительно удаленной от активных границ, представляют большой интерес с точки зрения определения источника тектонических деформаций и закономерностей их активизации во внутриконтинентальных условиях. Наши исследования были сосредоточены на части Юго-Восточной Монголии, в которой выделяются в разной степени активизированные на неотектоническом этапе мезозойские Восточно-Гобийская и Южно-Гобийская депрессии. Задача настоящей работы – оценка палеонапряженного состояния земной коры этой территории, выявление этапов и механизмов кайнозойской активизации структур разного простирания и определение ее источников. Сопоставление литературных данных о геологической истории развитии Восточно-Гобийской и Южно-Гобийской депрессий свидетельствует о единой истории развития территории в позднеюрско-раннемеловое (рифтообразование) и позднемеловое – палеогеновое время (режим тектонической стабилизации). На кайнозойском этапе эти впадины испытали совершенно различную по стилю активизацию. Помимо активизации левосторонними сдвигами в Восточно-Гобийской впадине в третичное время эта территория характеризуется развитием постпозднемеловых надвигов на ряде северо-восточных разломов в северном борту Тотошанского поднятия. Деформации позднемеловых осадков и реконструкции стресс-тензоров режима сжатия и транспрессии в зонах разломов свидетельствуют о субмеридиональном и СЗ сжатии в раннем кайнозое. Суммируя литературные данные, можно заключить, что наиболее вероятным источником этих деформаций могла быть Западно-Тихоокеанская зона межплитных взаимодействий. Нельзя также полностью отрицать возможность влияния процессов сжатия, происходивших на ранних стадиях в зоне Индо-Азиатской коллизии. Во второй половине кайнозоя эта территория была малоактивна. Активизация Южно-Гобийской депрессии в отличие от Восточно-Гобийской началась с позднего кайнозоя (конца миоцена – начала плиоцена). В этом районе происходит активное формирование рельефа с образованием молодых поднятий и форбергов (восточное окончание Гобийского Алтая), «протыкающих» осадки уже существовавших с мезозоя впадин. Эта территория характеризуется признаками плиоцен-четвертичной активности субширотных и СЗ сдвигов и надвигов. Реконструкции полей напряжений характеризуют режимы сжатия, транспрессии и сдвига с ориентировкой оси сжатия на северо-восток. Источником этих деформаций, так же как и деформаций структур Западной и Юго-Западной Монголии, являются процессы конвергенции Индостана и Евразии.

Ключевые слова: кайнозой; неотектоническая структура; палеостресс; активный разлом; Юго-Восточная Монголия

1. INTRODUCTION

Neotectonic structures in Southeastern Mongolia are an interesting object of studies aimed at establishing the regularities in activation of tectonic deformation in the intracontinental conditions. It is challenging to determine the source of deformation in this region located far away from the active borders of the lithospheric plates. Besides, the change in the strike of the main elements from W–E to northeastern was revealed in the ancient regional setting [*Badarch et al., 2002*]. Moreover, the modern terrain varies from mountains in the west (Gobi Altai) to weakly dissected flat areas in the east (Gobi plain). In the Late Cretaceous – Paleogene, the entire study area developed in condition of tectonic quiescence and terrain denudation, and the sediments of that period are overlying in most of the area [*Yanshin, 1975*]. Our study was carried out in Southeastern Mongolia with the focus on the East Gobi and South Gobi depressions originating from the Mesozoic and activated to various degrees in the neotectonic stage (Fig. 1).

The traces of the Cenozoic tectonic activity significantly differ in the studied depressions. The South Gobi depression was replaced by the mountains represented now by the eastern termination of Gobi Altai, including the Gurvan-Saikhan and Hurhe-Ula uplifts (Fig. 2, *a*), while low-amplitude linear uplifts and NE-trending basins developed within the limits of the East Gobi depression (Fig. 2, *b*).

The literature on the neotectonics of Southeastern Mongolia is still limited. The geology, Mesozoic and

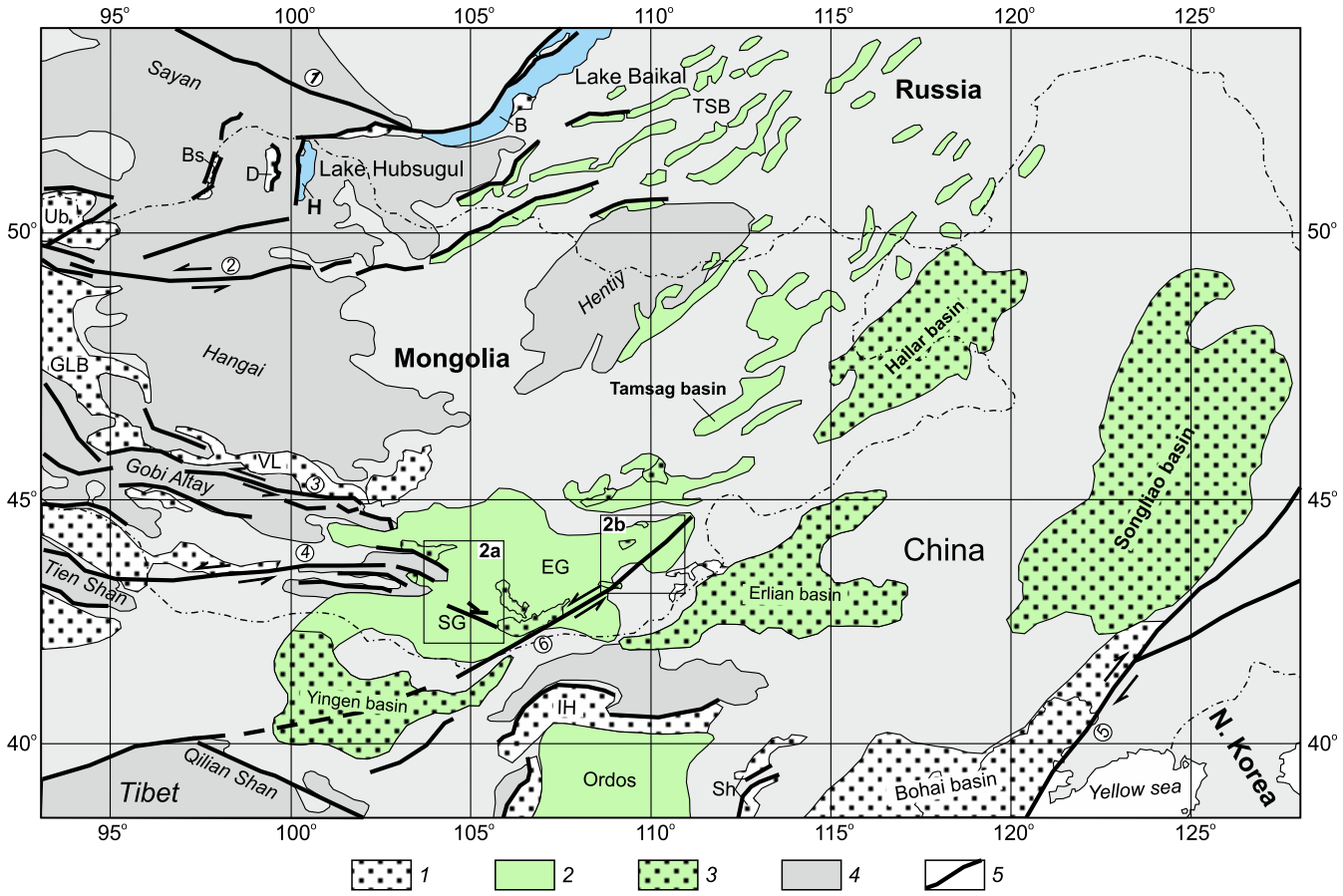

Fig. 1. Schematic tectonic map of Mongolia, the southern East Siberia and North China. Cenozoic basins: B – Baikal, H – Hubsugul, D – Darkhat, Bs – Busiyngol, Ub – Ubsunur, GLB – Great Lakes basins, Vl – Valley of Lakes, I-H – Inchuan-Hetao, Sh – Shanxi. Mesozoic basins: TSB – Transbaikalian system of basins, SG – South Gobi, EG – East Gobi. Faults (numbers in circles): 1 – Main Sayan, 2 – North Hangai, 3 – Gobi-Altai, 4 – Gobi-Tien Shan, 5 – Tanlu, 6 – East Gobi fault zone.

1–3 – basins filled with Cenozoic (*1*), Mesozoic (*2*), and Mesozoic–Cenozoic (*3*) sediments; *4* – uplifts; *5* – faults.

Рис. 1. Обобщенная тектоническая схема территории Монголии, юга Восточной Сибири и Северного Китая. Кайнозойские впадины: B – Байкальская, H – Хубсугульская, D – Дархатская, Bs – Бусийнгольская, Ub – Убсунурская, GLB – Котловина Больших Озер, Vl – Долиноозерская, I-H – Иньчуань – Хетао, Sh – Шаньси. Мезозойские впадины: TSB – Забайкальская система впадин, SG – Южногобийская, EG – Восточногобийская. Цифрами обозначены разломы: 1 – Главный Саянский, 2 – Северо-Хангайский, 3 – Гоби-Алтайский, 4 – Гоби-Тяньшанский, 5 – Танлу, 6 – Восточно-Гобийская разломная зона.

1–3 – впадины с кайнозойским (*1*), мезозойским (*2*) и мезокайнозойским (*3*) заполнением; *4* – поднятия; *5* – разломы.

Cenozoic tectonics and magmatism of Mongolia were investigated by the Soviet geologists in the mid 1950-60s [*Marinov et al., 1973; Yanshin, 1975*]. The studies of the neotectonics resumed in late 1990s, mainly for oil prospecting (e.g., [*Traynor, Sladen, 1995; Graham et al., 2001; Johnson, 2004; Webb, Johnson, 2006*]) and regional tectonic projects (e.g., [*Yue, Liou, 1999; Levi, 2007; Li et al., 2016*]). The neotectonic development history of Mongolia is still debatable. For instance, no significant strain is assumed in the neighboring Inner Mongolia after the Mesozoic stage of extension, according to the apatite fission-track analysis [*Li et al., 2016*]. However, other studies revealed clear indicators of moderate activation in the Cenozoic in East Gobi due to displacements along the NE-striking faults [*Yanshin, 1975; Webb, Johnson, 2006*]. Starting from [*Florensov, Solonenko, 1965*], various interpretations have been proposed for the Gobi-Altai structures that became widely known through the studies of the 1957 Gobi-Altai earthquake epicenter zone (M=8.1). In many publications on the Late Cenozoic and contemporary kinematics of faults, the geology and morphology of the Gobi Altai, it is viewed as a typical transpression structure formed in the regional strike-slip fault zone with a significant contribution of compression (e.g. [*Baljinnyam et al., 1993; Bayasgalan et al., 1999, Cunnihgham, 2007; Cunnihgham, 2013*]). According to [*Leonov, 2012*], the Gobi-Altai structures are intraplate zones of concen-

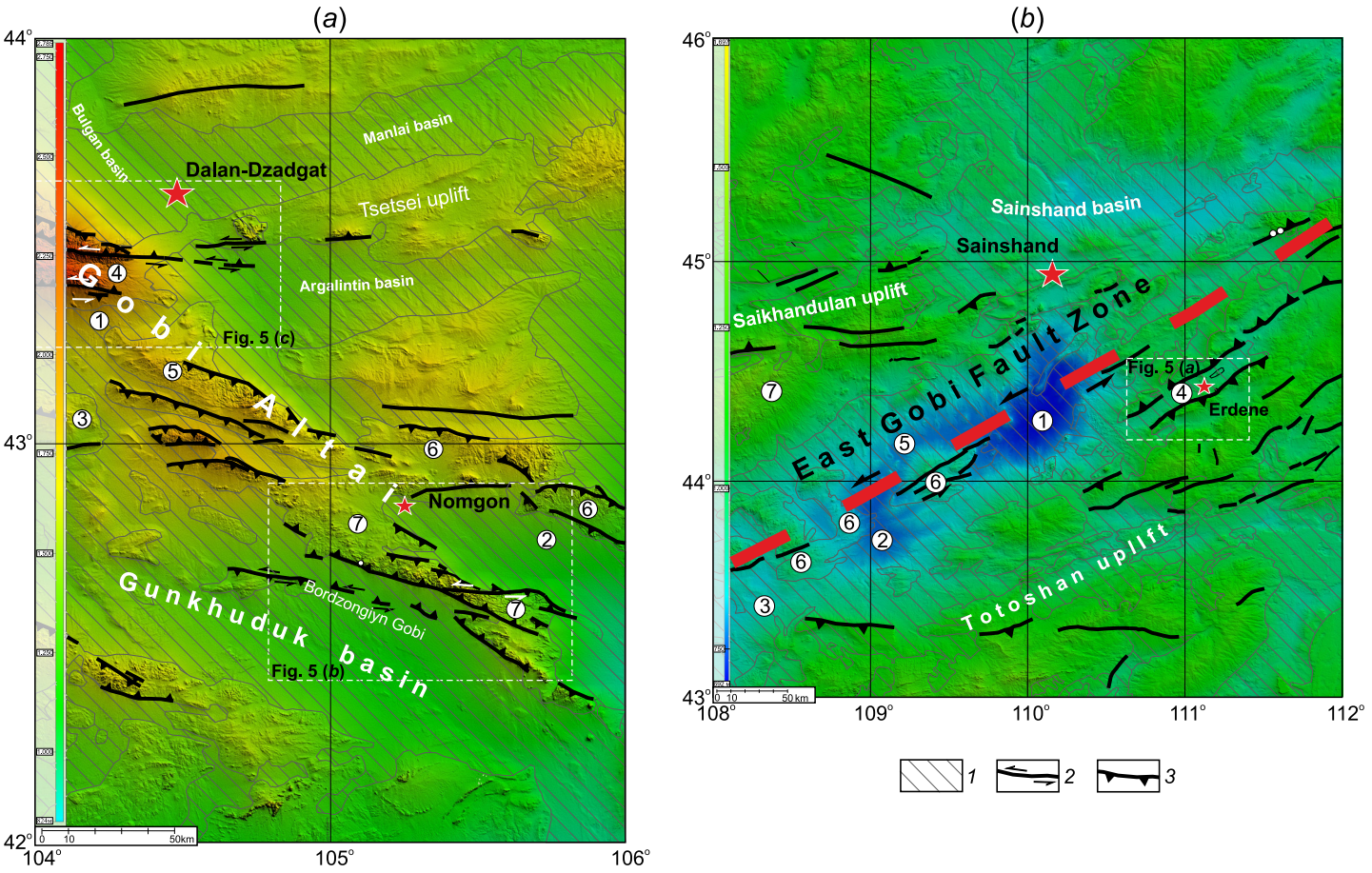

Fig. 2. Shaded relief SRTM-90 digital topography (http://www.nasa.gov) and active faults. (*a*) – South Gobi depression. Numbers in circles show basins and uplifts. Basins: 1 – Baindalai, 2 – Sangiyndalai. Uplifts: 3 – Dzurumtai, 4 – Gurvan–Saikhan, 5 – Buryn–Khar ridge, 6 – Yamata, 7 – Khurkhe-Ula ridge. (*b*) – East Gobi depression. Numbers in circles show basins and uplifts. Basins: 1 –Zuunbayan, 2 – Ulegei, 3 – Galbyngobi, 4 – Dalayn-Khanda, 5 – Unegt. Uplifts: 6 – TsaganSubarga, 7 – Mantakh.

1 – areas with platform cover sediments; *2* – strike-slip faults; *3* – thrusts.

Рис. 2. Схема активных разломов и цифровая модель рельефа SRTM-90 (http://www.nasa.gov). (*a*) – Южно-Гобийская депрессия. Цифрами в кружках обозначены впадины и поднятия. Впадины: 1 – Баиндалайская, 2 – Сангийндалайская. Поднятия: 3 – Дзурумтайское, 4 – Гурван-Сайхан, 5 – хр. Бурын-Хар, 6 – Яматинское, 7 – хр. Хурхэ-Ула. (*b*) – Восточно-Гобийская депрессия. Цифрами в кружках обозначены впадины и поднятия. Впадины: 1 – Дзунбаинская, 2 – Улэгейская, 3 – Галбынгобийская, 4 – Далайн-Хандийская, 5 – Унэгэтинская. Поднятия: 6 – Цагансубургинское, 7 – Мантахское.

1 – области распространения отложений позднемезозойско-кайнозойского чехла; *2* – сдвиги; *3* – надвиги.

trated strain that, as suggested by mapping, formed in transtension conditions, i.e. due to a combination of strike-slip faulting and extension.

The above-mentioned regions differ in the levels of modern seismic activity (Fig. 3). In the Gobi Altai, many high-magnitude earthquakes occurred, and their epicenters formed clusters along the main W-WS and E-SE-trending faults. In the Gobi plain, dissipated seismicity is dominant, and the recorded earthquake magnitudes do not exceed 5.6. The reconstructions show focal mechanisms of strike-slip, reverse fault, and reverse fault with strike-slip component. The reconstructed stress tensors for the modern stress field show that the Gobi Altai is dominated by transpression with the NE-SW-trending axis of maximum compression, while the Gobi plain (i.e. the eastern and NE areas) is under compression with the ENE-WSW-trending axis of maximum compression.

The study area is thus divided into the highly active western and low active eastern parts in the Late Cenozoic and the modern period. Considering the microplate tectonics of Asia mapped in [*Zonenshain, Savostin, 1979; Bird, 2002*], the eastern area is a part of the Amur lithospheric microplate, and the western zone belongs to the orogen. The presence of a larger submeridional structural boundary along approximately 95–105°E,

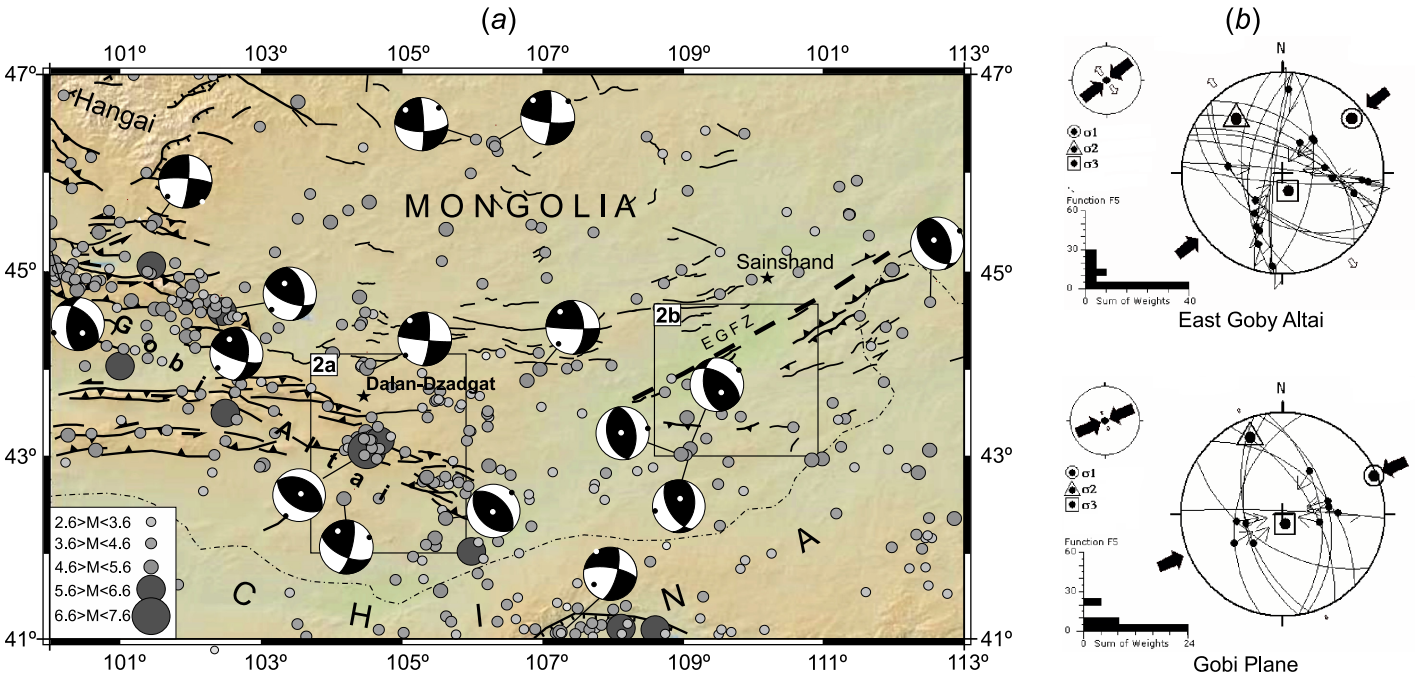

Fig. 3. Earthquake focal mechanisms (*a*) and present day stress state of SE Mongolia (*b*).

Рис. 3. Карта механизмов очагов землетрясений (*a*) и современное напряженное состояние Юго-Восточной Монголии (*b*).

which divides the entire continental Asia into the western and eastern parts, was proved by Semen I. Sherman in his publications on the modern geodynamics of Asia (e.g. [*Sherman et al., 2015, 2017*]). He stated that the main causes for the existence of this boundary included strong meridional compression due to the plate collision and the high rates of modern deformation in the western part, and lacking/less active collision processes in the eastern part.

Our study aimed to assess the paleostress state of the crust in Southeastern Mongolia, identify the stages, factors and mechanisms of the Cenozoic activation of the regional structures of different strike, and determine the sources of activation. In the first stage of investigations, we collected and processed the data on tectonic fracturing, displacements and morphotectonic features of active faults in the South Gobi and East Gobi depressions. In the second stage, local stress tensors were reconstructed and analyzed. The regional component of the stress field was indentified for different stages of development and compared with the published data on the Mesozoic-Cenozoic deformation of the adjacent territory of China.

2. Research Methods

The database on tectonic fracturing and tectonic deformation in the study area was consolidated using conventional geological, geomorphological, and geological-structural methods. Special attention was given to collecting the data on fault zones that were active in the Late Cenozoic and/or active at the modern stage. Initially, a map of active faults was compiled on the basis of satellite images and GTOPO-30, a global raster Digital Elevation Model (DEM). The map was then validated by field observations of the identified linear structures.

Dating of the fractures and deformations was challenging as most of the fracturing data was collected in the crystalline basement rocks, while outcrops of the Cenozoic rocks with easily traceable fractures were rarely observed. Fractures with calcite, zeolite and iron hydroxide (secondary mineralization) were considered indicative of subsurface conditions of their formation and, correspondingly, of the Late Mesozoic or Cenozoic age. Therefore, striations on the rocks with secondary mineralization can provide a basis for reconstructing the Cenozoic stress field. Besides, of great importance is dating of multidirectional striations on the same plane: the age relationships are used to distinguish the evolution stages of the stress field. In our study, striations on gouge in the rock crushing zones were considered as markers of the Cenozoic shear. Secondary mineralization, containing chlorite and epidote, was dated pre-Cenozoic and pre-Mesozoic due to its formation at depth. Accordingly, the reconstructed stress fields were dated pre-Cenozoic. The near-surface defor-

mations recorded in the active fault zones, such as the shifts of the valleys of temporary streams, deformations of the Cenozoic sediments, and etc. are also support for determining the Cenozoic stress fields.

Stress tensors were calculated from the tectonic fracturing data by TENSOR [*Delvaux, 1993*] and Win-TENSOR [*Delvaux, 2012*] software packages. The classification of stresses was based on values of coefficient R ($R=(\sigma_2-\sigma_3)/(\sigma_1-\sigma_3)$) that predetermines the shapes of stress ellipsoids and the stress ratios R' determining the stress regim [*Delvaux et al., 1997*].

3. The Late Mesozoic – Cenozoic geologic history of the study area

The paleogeodynamic reconstructions show that after the Mongol-Okhotsk (MO) Ocean closure due to the collision of the Northern Mongolian block and the Siberian plate at the turn of the Early – Middle Jurassic, a vast orogen was formed in the territory of the contemporary Transbaikalia, Mongolia and Northern China, and existed till the beginning of the Late Jurassic [*Zorin, 1999, Wang et al., 2012, Meng, 2003*]. In the Late Jurassic and Early Cretaceous, a system of depressions occurred from Transbaikalia and Mongolia and Northeastern China (see Fig. 1): the Transbaikalian system of basins, East Gobi, South Gobi, Tamtsag, Hailar, Erlian, Yingen and Songliao depressions. Some of the basins in Transbaikalia, Northeastern Mongolia and Northeastern China were accompanied by the formation of the metamorphic nuclei complexes. They bordered by gently dipping normal faults and have long and narrow boundaries (e.g. [*Wang et al., 2013; Zorin, 1999; Daoudene et al., 2009; Davis et al., 1996, 2002; Ritts et al., 2010; Mazukabzov et al., 2006, 2011; Sklyarov et al., 1997*]). Some basins, specifically the East Gobi, Songliao, Yangen, Erlian and Hailar, are described as rifts with thick sediments, which are bordered by steeply-dipping faults (e.g. [*Wang et al., 2012; Meng, 2003; Graham et al., 2001; Johnson 2004; Feng et al., 2010*]). According to [*Wang et al., 2012*], the Late Jurassic- Early Cretaceous extension was not took place simultaneously across the entire Northeastern Asia, but began in Mongolia and the China-Mongolia border areas and then spread into other regions in the southeast. To the west of this region, the territory belonging now to West China, West Mongolia and the Tien Shan was under compression due to collision processes at the southern boundary of Eurasia. From the Triassic to the Early Cretaceous, the collision between the Qiangtang, Lhasa blocks and Eurasia took place. In the Late Jurassic – Early Cretaceous, sedimentation occurred in ramp, foreland and pull-apart basins [*Caroll et al., 2010; Vincent, Allen, 1999; Johnson et al., 2015; Cunningham, 2013*]. At the same time, evidence of the Late Jurassic-Early Cretaceous rifting is found practically everywhere in the Gobi Altai. The intermountain depressions are filled with Jurassic-Cretaceous sediments, overlain by young Neogene-Quaternary sediments, and the Jurassic-Cretaceous deposits are uplifted and eroded in young ridges [*Cunningham et al., 2009; Cunningham, 2010, 2013; Horton et al., 2013*]. The passively uplifted Cretaceous normal faults were discovered in the Ih Bogt ridge of the Gobi Altai [*Cunningham, 2013*]. Extension within the modern Gobi Altai is also evidenced by metamorphic core complexes, such as an MCC exhumed by the Cenozoic uplift in the northwestern part of the Altan Uul ridge [*Cunningham et al., 2009; Cunningham, 2013*], and the Yagan Onch Hairhan MCC at the southern border of Mongolia and China [*Webb et al., 1999*]. According to the recent publications, the Valley of Lakes, in particular its northeastern part covered by seismic surveys, was also involved in rifting in the Late Jurassic – Early Cretaceous, and the accumulated sediment thickness amounted to 4–5 km. It is suggested that this Mesozoic depression formed due to transtension. Starting from the Neogene, transpression, folding and reverse thrusting on normal faults took place in this region [*Constenius et al., 2013; Johnson et al., 2015*]. Extension and rifting in the Late Jurassic – Early Cretaceous and the inversion of the regime in the Late Cenozoic was discovered up to the southern Mongolian Altai, including the Dzereg, Dariv and Shargiin Gobi basins [*Howard et al., 2003, 2006; Cunningham, 2013*]. However, the NW orientation of these basins may be questioned, considering rifting at the background of general NW extension.

In some publications, the final closure of the MO Ocean is shifted to the Late Jurassic–Early Cretaceous, and extension is excluded from that period. In the Late Jurassic, the MO Ocean was not completely closed, as shown by the paleomagnetic studies of the Upper Jurassic basalts from the volcanic tectonic structures of Transbaikalia and the calculations of the paleomagnetic pole of rotation [*Metelkin et al., 2007*]. It should be noted that the authors make a reservation that the difference in the positions of the Middle–Late Jurassic paleomagnetic poles of Northern China and Mongolia and South Siberia may be due to not only of the open MO Ocean, but also the contraction and deformation of the continental crust during the collision [*Metelkin et al., 2007*]. Based on the AFT analysis, *Van Der Beek et al.* [*1996*] relate the phase of rapid cooling in the Early Cretaceous and, accordingly, uplifting in the Baikal region and Transbaikalia to the Late Jurassic–Early Cretaceous orogeny caused by the final closure of the MO Ocean. They associate the exhumation of MCC in Transbaikalia with the same phase. Based on the paleostress reconstructions from the data on tectonic fracturing of the Early Cretaceous rocks in Transbaikalia, the stage of N-S compression was identified

[*Delvaux et al., 1995*]. This stage was dated to the Late Jurassic – Early Cretaceous and also associated with the closure of the MO Ocean and the formation of the orogen. However, later publications on Southeastern Mongolia and Northeastern China consider the inversion stage with the NW-trending compression at the turn of the Early and Late Cretaceous [*Graham et al., 2001; Johnson, 2004*].

The source of the Late Jurassic – Early Cretaceous extension remains a topic of debate. Some publications explain it by back-arc spreading due to the Paleo-Pacific plate subduction westwards underneath the Asian continent (e.g. [*Traynor, Sladen, 1995; Watson et al., 1987*]). Most researchers, however, relate the extension to the gravitational collapse of the Middle Jurassic orogen (e.g. [*Zorin, 1999; Wang et al., 2012; Meng, 2003*]). *Q.-R. Meng* [*2003*] proposed a model combining the gravitational collapse of the orogen and active rifting and stated that active rifting took place as a result of the subduction and separation of the Mongol-Okhotsk oceanic plate slab pushed underneath the Siberian continent. The latter in its turn, caused extension and weakening of the lithospheric bottom of the Mongolia-North China block, ascending asthenospheric flows, melting of the mantle and crust, extensive volcanism and magmatism, as well as active formation of the rift basins bordered by gently dipping listric faults. In the Late Cretaceous and Paleogene, the study area was in tectonic quiescence, with gradual post-rifting subsidence in the basins and planation of the existing terrain. The next stage of tectonic activation is related to the collision of the Indian and Eurasian plates and the development of the modern mountain systems and depressions [*Cunningham, 2007, 2010, 2013*].

Our study was focused on the Mesozoic East and South Gobi depressions located in Southeastern Mongolia (see Fig. 1 and 2). As mentioned above, in the Late Jurassic – Early Cretaceous, rifting took place in the East and South Gobi depressions; the basins were formed, and the sediments were accumulated [*Graham et al., 2001; Johnson, 2004*].The development of the basins was accompanied by extensive volcanic activity that generated the terrigenous sedimentary strata containing a large amount of volcanic material. In total, the thickness of the Late Jurassic – Early Cretaceous sediments in the East Gobi depression varies from 1.0 to 3.0 km [*Yanshin, 1975*]. The NE strike of the structure-forming rift-related faults in this depression suggests the NW extension in the Late Jurassic – Early Cretaceous. The analysis of seismic profiles across the Dzunbai and Uneget basins (East Gobi depression) [*Johnson, 2004*] shows that the development of the basins was inverted when sedimentation ceased at the turn of the Late Jurassic – Early Cretaceous, and resulted in folding and reverse thrusting of the synrift sediments that were later overlain by non-deformed Upper Cretaceous and Cenozoic sediments. Some of the rift-related faults experienced reverse overthrusting. Folding deformation of the Late Jurassic – Early Cretaceous sediments is also observed in the South Gobi depression [*Yanshin, 1975*]. At the turn of the Early – Late Cretaceous, compression could have occupied a wider area, as evidenced by the folds in the Late Jurassic–Early Cretaceous sediments in other Cretaceous basins of Mongolia and China, e.g. the Songliao basin in Northeastern China [*Graham et al., 2001*] and the Baganur basin in the southern part of the Hentei dome [*Dill et al., 2004*].The NW-N-S compression is evidenced by the trends of the fold axes and activated reverse faults.

The Late Cretaceous sedimentation is associated with post-rift thermal sinking [*Johnson, 2004*]. Starting from the end of Cretaceous and in the Paleogene, the study area was in tectonic quiescence, the terrain was denudated, and the accumulation of sediments was moderate. The Upper Cretaceous and Cenozoic sediments are positioned sub-horizontally with an angular unconformity on the eroded surface of the Late Jurassic – Early Cretaceous sediments. Their thickness, varying from 150–200 m to 500–700 m, is significantly less than the thickness of the synrift sediments [*Yanshin, 1975*]. The Cenozoic sediments are less thick and less abundant than the Upper Cretaceous ones. In addition to the Quaternary and recent sediments, the Cenozoic section is mainly represented by the Paleocene, Eocene and Lower Oligocene sediments. A distinctive feature of the Upper Cretaceous sediments is their red colour. The sediments are of the polyfacial genesis and include proluvial, lacustrine, alluvial and lacustrine-alluvial deposits with thin layers of basalts. The Paleogene sediments are of the lacustrine, alluvial and lacustrine-alluvial origin and have variegated and red colors.

The distribution of the sediments of the Upper Cretaceous-Paleogene cover reveals the Gobi basin, which occupies the entire southeastern and southern part of Mongolia and extends southward to the territory of China [*Yanshin, 1975*].The South Gobi depression includes the Bulgan, Argalintin, Baindalai, Sangindalai, Gunkhuduk, and Manlai basins and the Gurvansaikhan, Khurkha, Tsetsei, Dzurumtai, and Yamata uplifts (see Fig. 2, *a*).The NW and W-E trends are most typical of these structures. In the East Gobi depression (see Fig. 2, *b*), the largest structures are the Saishand, Unegt, Zuunbayan, Ulegei, and Galbyn-Gobi basins separated by the Mantakh, Saikhandulan, Tsagan Subarga and Totoshan uplifts. These structures trend in the NE and W-E directions.

Most uplifts in Southeastern Mongolia are syndepositional and represented by the sedimentation source areas, and the modern relief is plain-hilly. However, some of these uplifts are either newly formed in the Late Cenozoic (i.e. the recent stage) or have been activated and involved in the recent uplifting. The new/ac-

tivated uplifts are characterized by the high- or low-mountain, strongly dissected relief and bordered by faults. In the study area, such structure is the eastern termination the Gobi Altai, including the Gurvan-Saikhan, Buryn Har and Hurhe Ula ridges. The Gobi Altai is described in [*Cunningham, 2007, 2010, 2013*] as the intracontinental transpression mountain building zone, and its eastern termination is viewed as a restraining bend of horsetail splay termination zone of the largest and longest Gobi-Tien Shan fault zone.

The Alpine-type relief Gurvan-Saikhan ridge separates the Bayandalai and Bulgan basins. According to [*Yanshin, 1975*], these basins developed from the single structure in the Late Cretaceous – Paleogene, as evidenced by the similar sedimentation sections of both basins and the lack of facial changes in the Upper Cretaceous – Paleogene sediments in the vicinity of the ridge. The newly formed structure is the large part of the Khurkh-Ula range (the Khurkhan uplift), as evidenced by the strongly dissected relief, antecedent valleys cutting through the ridge and the Lower and Upper Cretaceous deposits in its southeastern part, raised and dislocated on the sides of the ridge. Recent activity at the edges of the Tsetsei, Dzurumtai and Yamata uplifts is evidenced by clear fault scarps on their sides. In South Gobi depression, the Late Cenozoic activation is poorly manifested, and most of its uplifts are syndepositional. The traces of the Cenozoic activity are revealed only at the Totoshan [*Yanshin, 1975*] and Tsagan Subarga [*Graham et al., 2001; Johnson, 2004; Webb, Johnson, 2006; Yue, Liou, 1999*] uplifts. The Tsagan Subarga uplift is dissected in its central part, and the southern side of its western half and the northern side of its eastern half are bordered by the East Gobi fault zone (EGFZ) originating from the Mesozoic, which currently separates the Unegta and Zuunbayan basins.

4. Analysis of fault structures, and stress field reconstructions

4.1. The East Gobi depression

Our field observations were focused on the sides of the small Dalain-Khunda basin located east of EGFZ and the faults bordering the small ridges of the Totoshan uplift (Fig. 4, *a*, and Fig. 5). In this area, the main structures are NE-trending. Practically all the studied local fault zones show reverse faulting and thrusting of the crystalline basement over the Upper Cretaceous red beds that fill the basin. One of the NE-trending scarps located north of Erdene Somon (Fig. 5, *a*, and Fig. 6, *a*) is the basin's northern border. The main fault planes along the scarp have a north-western and a northern dip at angles from 25° to 45°. The fragmented cataclastic crystalline rocks (crystalline schists and pegmatites) thrust onto the Upper Cretaceous red sediments (argillites) (Fig. 6, *b*). In the contact zones, the red sediments were thermally hardened as a brick. By reconstructing the stress tensors for the outcrops located in the contact zones, compression regime with the N-S-trending axis of the maximum compression is revealed, as well as strike-slip regime with the WNW-ESE-trending axis of maximum compression (Fig. 7, *a*, *b*, *c*; Table). For the rear side of the thrust, the subhorizontal Lower Cretaceous sediment layers (interbedded brown, yellowish-brown sandstones, conglomerates, and gravelites) and the crystalline basement rocks show the relationships of two types. The sediments overlay the crystalline basement rocks at low angles, and, at the same time, there is a steep tectonic contact (340°∠80°) that may represent a rift-forming fault on the ground surface. Based on the analysis of tectonic fracturing, the NW-trending extension regime is reconstructed for this zone (Fig. 7, *d*; see Table).

The scarp bordering the southern side of the basin strikes NE to ENE (see Fig. 4, *a*, and Fig. 5, *b*, *c*, *d*). Practically everywhere along this scarp, the crystalline basement rocks thrust onto the Upper Cretaceous red sediments (sandstones, gravelites, and conglomerates) (see Fig. 6, *c*, *d*, *e*, and Fig. 8, *a*, *b*, *c*, *d*, *e*). The dip direction of the main fault planes vary from 120°–150° to 180° with the change of the scarp's strike from western fault segment to eastern one. Both reverse- (Fig. 8, *d*, *e*) and thrust-type displacements (Fig. 8, *a*, *b*) are observed along the fault zone, and the dip angles change from steep to very low-angle. Cataclasites, tectonic breccias (kakirites), zones of rock crushing (to tectonic flour), gouge, and thin weathering gouge layers are typical for the contract zones (Fig. 6, *e*, and Fig. 8, *b*, *e*). In some places, the sediment layers are turned up underneath the thrust plane, and the layers dip at angles varying from 1–2° at a distance from the contact to 30–45° directly at the contact (N and NW dip). No evident strike-slip displacements were observed in the fault zones. The stress field reconstructions show mainly compression and transpression regimes with the NW and N-S axes of compression (Fig. 7, *f*, *g*, Fig. 9, *a*, *b*, *d*, *e*, *f*; see Table). There are a few reconstructions of strike-slip and compression regimes with the NE axes of compression (Fig. 7, *e*, Fig. 9, *c*; see Table). Due to the fact that the Upper Cretaceous red sediments are displaced, but there is no deformation of the Cenozoic sediments, the upper age limit for the observed deformation cannot be specified, while the lower limit may be dated as the post-Late Cretaceous. The Cenozoic age of the basin is suggested by the fact that the propagation of the Upper Paleogene sediments was controlled by the faults bordering the basin, and the border scarp are quite straight and weakly eroded. The indicators of the Late Cenozoic activity are traceable east of Erdene Somon wherein the local erosional network is actively

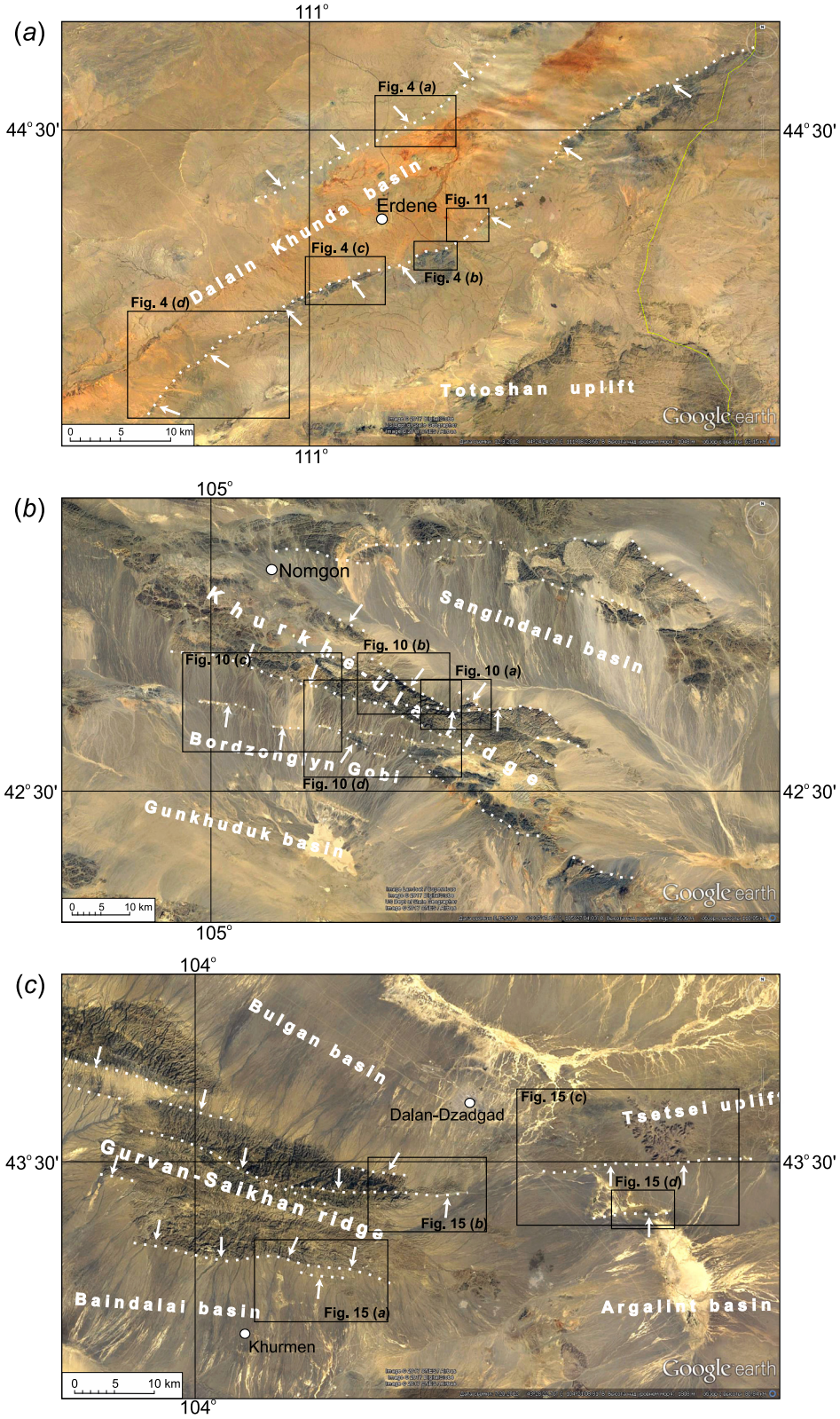

Fig. 4. Spot (Google Earth) satellite images of the study area: (*a*) – Erdene Somon vicinities (East Gobi depression), (*b*) – NomgonSomon vicinities (South Gobi depression); (*c*) – Dalan-Dzadgad vicinities (South Gobi depression). Fault scarps are shown by dashed lines and arrows. Locations of (*a*), (*b*) and (*c*) images are shown in Fig. 2. Positions of Fig. 5 (*a*), (*b*), (*c*), (*d*), Fig. 10, Fig. 11 (*a*), (*b*), (*c*), (*d*) and Fig. 16 (*a*), (*b*), (*c*), (*d*) are shown by boxes.

Рис. 4. Обзорные космические снимки «Spot» (Google Earth) районов исследований: (*a*) – окрестности сомона Эрдэнэ (Восточно-Гобийская депрессия); (*b*) – окрестности сомона Номгон (Южно-Гобийская депрессия); (*c*) – окрестности г. Далан-Дзадгад (Южно-Гобийская депрессия). Уступы активных разломов обозначены пунктирными линиями и стрелками. Положение рисунков (*a*), (*b*), (*c*), (*d*) показано на рис. 2. Прямоугольниками показано расположение рис. 5 (*a*), (*b*), (*c*), (*d*), рис. 10, рис. 11 (*a*), (*b*), (*c*), (*d*), рис. 16 (*a*), (*b*), (*c*), (*d*).

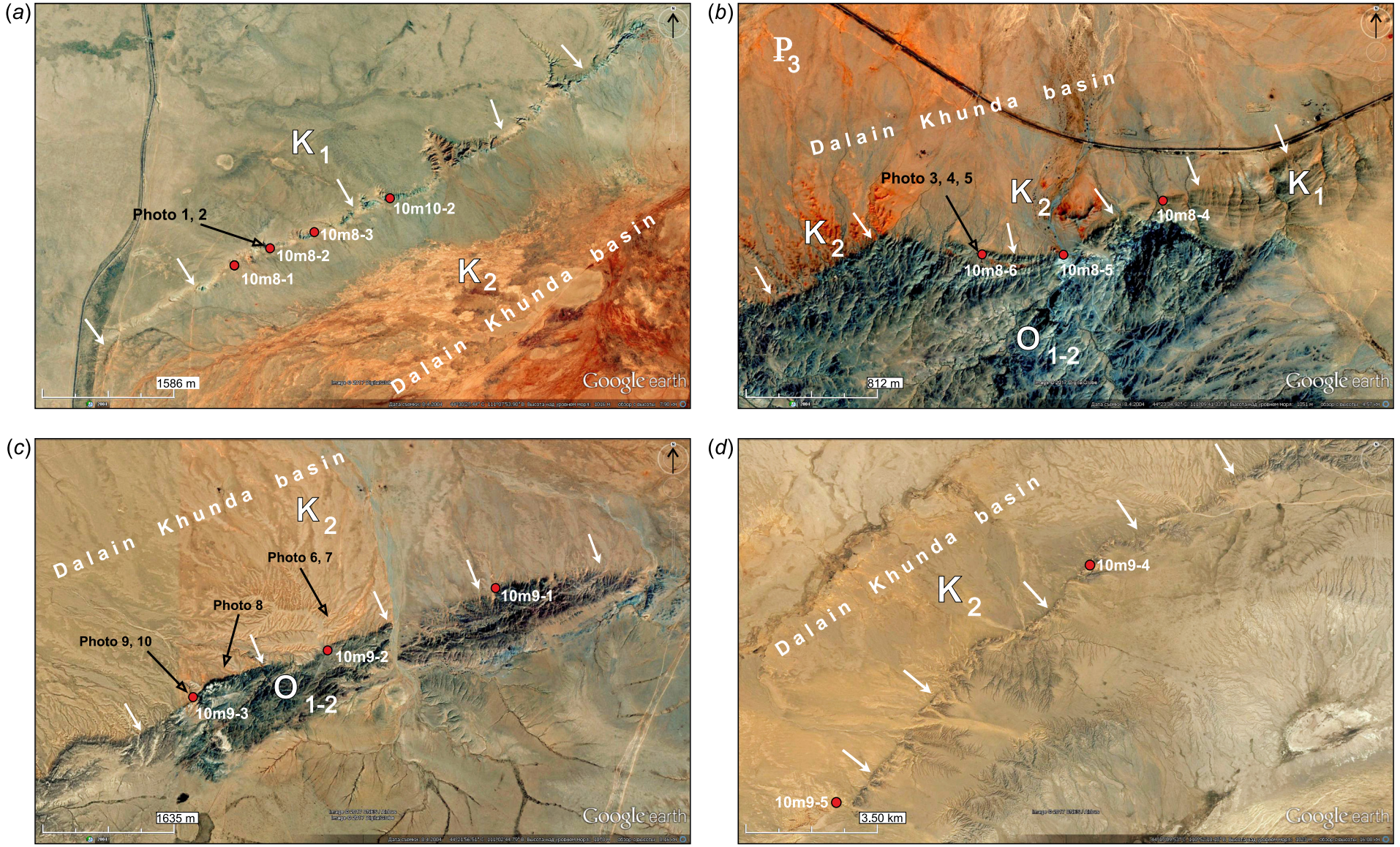

Fig. 5. Fragments of Spot (Google Earth) satellite images of Cenozoic faults bordering the Dalain-Khunda basin in the East Gobi depression. Locations of (*a*), (*b*), (*c*), and (*d*) images are shown in Fig. 4. Observation points are marked by red circles and corresponding code numbers.

Рис. 5. Фрагменты космических снимков «Spot» (Google Earth), показывающие кайнозойские бортовые разломы Далайн-Хундийской впадины (Восточно-Гобийская депрессия). Положение рисунков (*a*), (*b*), (*c*), (*d*) показано на рис. 4. Красными точками обозначены пункты наблюдения с соответствующим кодовым номером.

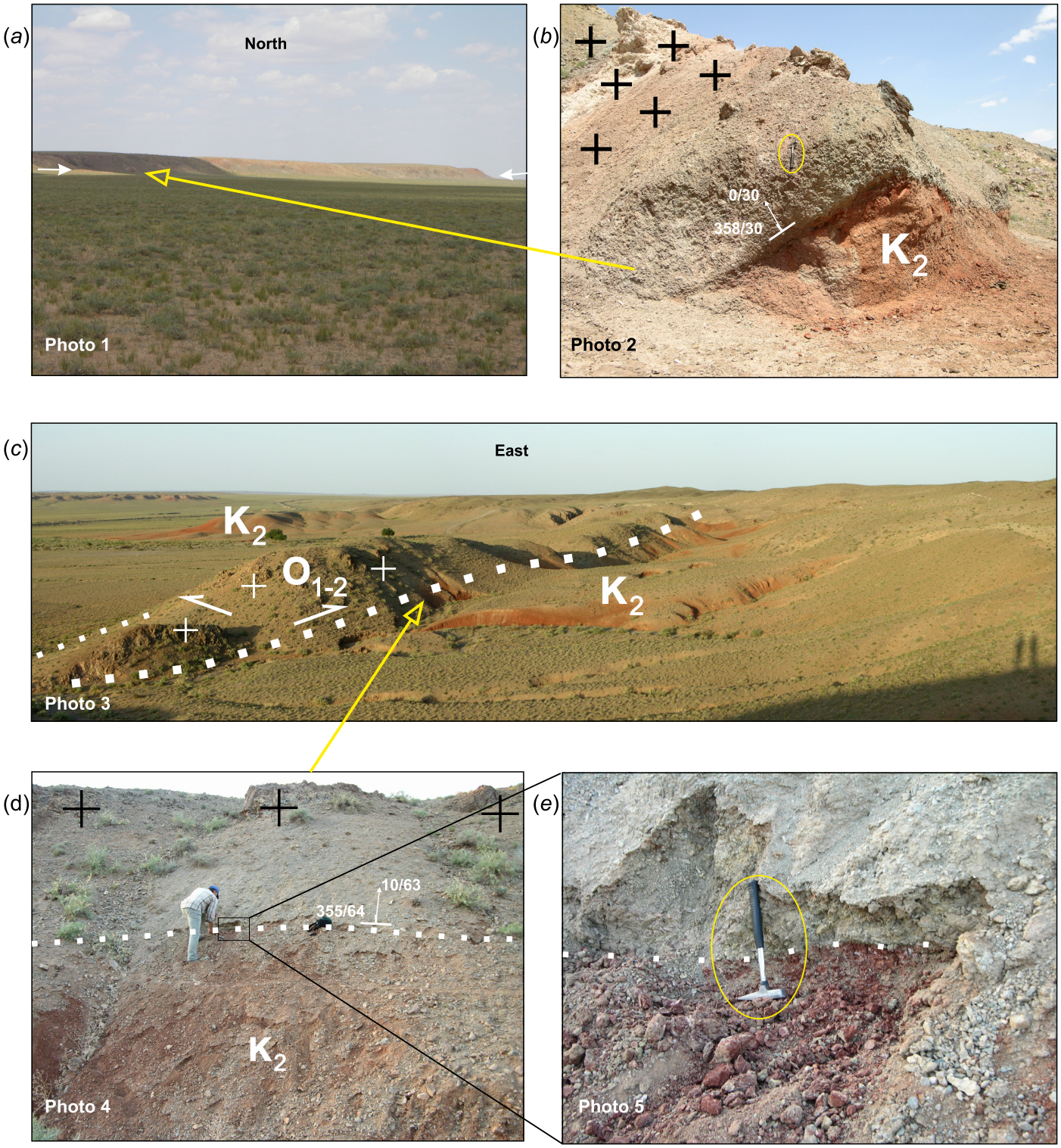

Fig. 6. Cenozoic deformation near the northern fault bordering the Dalain–Khunda basin (north of Erdene Somon): (*a*) – view of the scarp from south, (*b*) – thrust contact of the crystalline basement rocks and Upper Cretaceous sediments; (*c*), (*d*), (*e*) – Cenozoic deformation near the southern fault bordering the Dalain–Khunda basin (south of Erdene Somon): (*c*) – view of the scarp, (*d*) – thrust contact of the crystalline basement rocks and Upper Cretaceous sediments, (*e*) – weathering gouge zone at the contact. See the locations in Fig. 5.

Рис. 6. Кайнозойские деформации в зоне северного бортового разлома Далайн-Хундийской впадины (к северу от сомона Эрдэнэ): (*a*) – вид на уступ с юга, (*b*) – надвиговый контакт пород кристаллического основания и верхнемеловых отложений; (*c*), (*d*), (*e*) – кайнозойские деформации в зоне южного бортового разлома Далайн-Хундийской впадины (к югу от сомона Эрдэнэ): (*c*) – вид на уступ, (*d*) – надвиговый контакт пород кристаллического основания и верхнемеловых отложений, (*e*) – кора выветривания в зоне контакта. Местоположение фото показано на рис. 5.

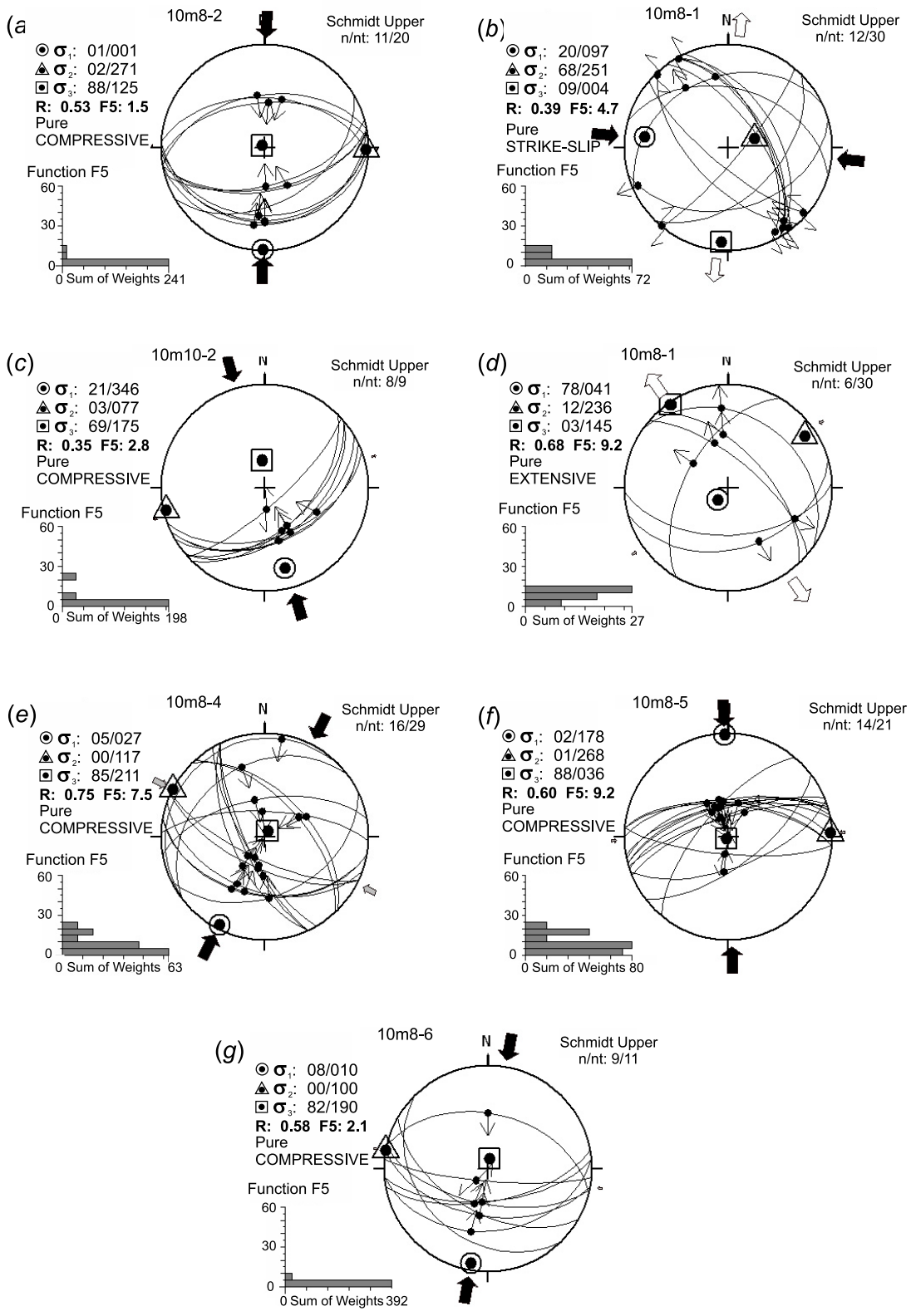

Fig. 7. Paleostress reconstructions for fault zones in the Dalain–Khunda basin. Stereograms – Wulff net, upper hemisphere. Histograms show deviations (p) of the observed slip from theoretical slip values for each fault plane. Circle – compression axis, σ_1; triangle – intermediate axis, σ_2; square – extension axis, σ_3. Numbers show dip angle and azimuth of the respective axes of main normal stresses. The numbers of stress tensors correspond to the numbers of observation points in Fig. 5.

Рис. 7. Реконструкции палеонапряжений в зонах разломов Далайн-Хундийской впадины. Стереограммы – сетка Вульфа, верхняя полусфера. Гистограммы показывают отклонения (p) наблюдаемого скольжения от теоретического для каждой плоскости разрыва. Кружком обозначена ось сжатия σ_1, треугольником – промежуточная ось σ_2, квадратом – ось растяжения σ_3. Цифрами обозначены угол падения и азимут падения соответствующих осей главных нормальных напряжений. Номер стресс-тензора соответствует номеру точки наблюдения на рис. 5.

developing. On the 2.5×3.0 km site at the southeastern side of the Dalayn-Khunda basin, we observed a new network of small gullies in the center and dry washes (locally named 'sairs') cutting the perimeter of the low-amplitude uplift (Fig. 10). On the same site, along layer detachment was observed in the gently dipping Upper Cretaceous red sediments (Fig. 8, *f*).The stress field reconstruction shows transpression regime with the N-S-trending axis of maximum compression (Fig. 9, *h*; see Table).

4.2. The South Gobi depression

We studied fault zones bordering the Gurvan-Saikhan and Khurkhe-Ula ridges, some small ranges and forebergs in the surrounding areas, as well as active fault zones traceable in the inner field of the Gunkhuduk basin (Fig. 4, *b*, *c*).

The NE and SW sides of the NW-trending Khurkhe uplift are bordered by faults (Fig.4, *b*, and Fig. 11). Besides the NW-striking faults, we observed the W-E faults, the largest of which goes across the central part of the Khurkhe-Ula ridge (Fig. 11, *a*). In this fault zone, the left-lateral displacements of temporary water stream valleys amount to 30–35 m (Fig. 12, *a*). The fault is steeply dipping, 80 to 90°, and its main plane dips to S and S-SW. The stress field reconstructions for the observation points along this fault zone show strike-slip conditions regime with the NE-trending axis of compression (Fig. 13, *a*, *b*, *c*; see Table).

Our studies of the NE slope of the Khurkhe-Ula ridge, that borders the Sangindalai basin (see Fig. 11, *a*, *b*), revealed mainly thrust-type and reverse displacements along the NW-striking faults (Fig. 12, *b* to *g*). The faults are marked by cataclastic and crushed rocks and weathering gouge (Fig. 12, *c*, *g*). The bordering fault planes dip in the SW direction, underneath the ridge, at the angles from 45° to 85°. In some places, we observed the crystalline basement thrust onto the Mesozoic (Cretaceous) sediments. A thrust of granite onto loose conglomerates was discovered near the Mogoin-Khuduk site (Fig. 12, *b*, *c*, *d*). The S-SW dipping thrust plane is accompanied by a linear weathering gouge zone (to 2 m thick), and its dip angle ranges from 30° to 18° (Fig. 12, *c*). In the same area, the Mesozoic conglomerates overthrust onto the Quaternary terrace, and the fault plane dips at 225°∠67°. Along the SW side of the Sangiyndalai basin, there are dry water stream valleys with weakly cemented sandstones, conglomerates and gravelites, which are disturbed by steeply dipping rock crushing zones and along layer disruptions, with obvious reverse displacements at some locations (Fig. 12, *h*). The fault planes dip to SW (the dip azimuth of 215–230°) at the angles of 58–75°. As we approach the sides of the basin, we observe the twisting of sedimentary layers (the dip azimuth of 185–220° with the angles from 28 to 65°). For the fault zones at the NE side of the Khurkhe-Ula ridge, the stress field reconstructions show transpression, compression and strike-slip regimes with the dominating NE trend of maximum compression (Fig. 13, *d* to *k*; see Table 1). The SW side of the Khurkhe uplift is clearly bordered by the fault (Fig. 11, *c*). Based on the tectonic fracturing in the Paleozoic rock outcrops along the NW-striking scarp, the stress field reconstruction shows compression and strike-slip regimes with the NE-trending axis of compression (Fig. 14, *a*, *b*, *e*, *f*; see Table).

The Gunkhuduk basin is located south of the Khurkhe-Ula ridge. On the Bordzongiyn Gobi site located at the northern side of this basin, we observed a series of W-E and NW-trending scarps that deform the gently sloping plain (see Fig. 4, *b*, Fig. 11, *c*, *d*, and Fig. 15, *a* to *d*). Practically everywhere near the scarps, there are the outlets of relatively large water springs. The north wall of the fault is uplifted. The scarp height varies from 0.5 to 1.3 m along the strike. The left-lateral shear amplitude of the dry water stream valleys ranges from to 1.5 to 9.0 m (Fig. 15, *b*, *c*). Further eastward, this series of scarps is conjugated with the faults bordering the SW side of the Khurkhe-Ula ridge. The stress field reconstructions for several Paleozoic rock outcrops along the scarp show compression, transpression and strike-slip conditions regimes with the NE and N-S axes of compression (Fig. 14, *c*, *d*, *g*, *h*; see Table).

Our studies of active faults bordering the Gurvan-Saikhan uplift were carried out in its eastern termination near the town of Dalan-Dzadgad (see Fig. 4, *c*, and Fig. 16). At the southern side of the uplift, there is the W-E fault zone north of the Khurmen Somon, wherein we observed a well-defined scarp that is generally trending at 295° (Fig. 16, *a*). The fault zone along the scarp is marked by tectonites, mylonites, tectonic breccias (kakirites), and higher density of fractures. Its total thickness is not less than 500 m. The fault is rather steeply dipping (70–80°). Along the strike of the scarp, the local water stream valleys are left-laterally shifted by 100–150 m. The foreberg located further to the south and penetrating the northern side of the Baindalai basin, is clearly bordered at the north by the faults, which main planes dip to the south (Fig. 16, *a*, and Fig. 17, *a*). The stress field reconstructions for these fault zones shows strike-slip, transpression and compression regimes with the NE-trending axis of compression (Fig. 18, *a* to *e*; see Table).

Resent (Holocene) deformations were revealed in the eastern termination of the Gurvan-Saikhan uplift (Fig. 16, *b*; Fig. 17, *b*, c). In this area, at the southern slope of the small W-E foreberg, we observed the thrust of mylonitized basic rocks onto the Quaternary diluvium sediments of the slope (Fig. 17, *b*). The fault zone is marked by a linear weathering gouge zone. The main fault planes dip to N and NE at the angles of 65–44°.

Paleostress reconstruction results

Результаты реконструкций палеонапряжений

Site	Long	Lat	Location	Stratigraphy	Structure	n	nt
1	2	3	4	5	6	7	8
10m8-1a	111 06 45.6	44 30 04.5	Erdene		nothern Dalain-Khunda fault	12	30
10m8-1b	111 06 45.6	44 30 04.5	Erdene		nothern Dalain-Khunda fault	6	30
10m8-2	111 07 04.6	44 30 10.4	Erdene	Upper Cretaceous	nothern Dalain-Khunda fault	11	20
10m8-4	111 10 08.1	44 23 36.0	Erdene	Lower Cretaceous	southern Dalain-Khunda fault	16	29
10m8-5	111 09 42.1	44 23 26.0	Erdene		southern Dalain-Khunda fault	14	21
10m8-6	111 09 19.0	44 23 24 .9	Erdene		southern Dalain-Khunda fault	9	11
10m9-1a	111 04 00.1	44 22 19.3	Erdene		southern Dalain-Khunda fault	14	33
10m9-1b	111 04 00.1	44 22 19.3	Erdene		southern Dalain-Khunda fault	6	33
10m9-2	111 02 25.7	44 21 59.9	Erdene		southern Dalain-Khunda fault	14	22
10m9-3	111 01 13.4	44 21 38.4	Erdene		southern Dalain-Khunda fault	5	13
10m9-4	110 52 40.5	44 18 08.6	Erdene	Upper Cretaceous	southern Dalain-Khunda fault	28	30
10m9-5	110 47 50.7	44 14 52.8	Erdene	Upper Cretaceous	southern Dalain-Khunda fault	20	21
10m10-1	111 12 06.6	44 25 07.7	Erdene	Upper Cretaceous	southern Dalain-Khunda fault	6	16
10m10-2	111 08 05.6	44 30 28.4	Erdene	Upper Cretaceous	southern Dalain-Khunda fault	8	9
11m3-1a	105 30 06.7	42 37 51.2	Nomgon		W-E Khurkhe-Ula fault	18	64
11m3-1b	105 30 06.7	42 37 51.2	Nomgon		W-E Khurkhe-Ula fault	10	64
11m3-2	105 30 28.7	42 37 47.6	Nomgon		W-E Khurkhe-Ula fault	20	28
11m3-4	105 33 24.8	42 38 34.3	Nomgon		NW Sangindalai thrust	12	19
11m3-5	105 33 31.7	42 38 30.9	Nomgon		NW Sangindalai thrust	10	23
11m4-1	105 29 39.2	42 38 21.6	Nomgon		NW Sangindalai fault	19	31
11m4-2	105 24 54.8	42 40 10.7	Nomgon		NW Sangindalai fault	25	41
11m4-3a	105 23 56.1	42 40 39.7	Nomgon		NW Sangindalai fault	11	47
11m4-3b	105 23 56.1	42 40 39.7	Nomgon		NW Sangindalai fault	14	47
11m4-4	105 22 18.4	42 42 36.9	Nomgon	Cretaceous	NW Sangindalai fault	15	17
11m4-5	105 21 02.6	42 44 18.1	Nomgon		NW Sangindalai fault	7	8
11m5-1a	105 06 04.8	42 41 56.4	Nomgon		NW Khurkhe-Ula fault	32	58
11m5-1b	105 06 04.8	42 41 56.4	Nomgon		NW Khurkhe-Ula fault	9	58
11m5-2	105 01 28.4	42 38 20.0	Nomgon	Quaternary	W-E Bordzongiyn Gobi fault	11	29
11m5-3	105 01 52.2	42 38 12.4	Nomgon		W-E Bordzongiyn Gobi fault	9	13
11m5-4a	105 06 05.0	42 42 04.9	Nomgon		NW Khurkhe-Ula fault	10	32
11m5-4b	105 06 05.0	42 42 04.9	Nomgon		NW Khurkhe-Ula fault	8	32
11m6-3a	105 18 30.1	42 34 54.7	Nomgon		W-E Bordzongiyn Gobi fault	18	45
11m6-3b	105 18 30.1	42 34 54.7	Nomgon		W-E Bordzongiyn Gobi fault	7	45
11m7-1a	104 09 03.6	43 23 16.6	Dalan Dzadgad		W-E southern Gurvan-Saikhan fault	5	53
11m7-1b	104 09 03.6	43 23 16.6	Dalan Dzadgad		W-E southern Gurvan-Saikhan fault	15	53
11m7-2a	104 10 14.7	43 23 02.6	Dalan Dzadgad		W-E southern Gurvan-Saikhan fault	11	29
11m7-2b	104 10 14.7	43 23 02.6	Dalan Dzadgad		W-E southern Gurvan-Saikhan fault	5	29
11m7-3	104 11 27.9	43 22 24.1	Dalan Dzadgad		W-E Gurvan-Saikhan foreberg	11	17
11m8-1a	104 20 13.1	43 28 00.0	Dalan Dzadgad		W-E Gurvan-Saikhan fault	18	34
11m8-1b	104 20 13.1	43 28 00.0	Dalan Dzadgad		W-E Gurvan-Saikhan fault	4	34
11m8-2	104 19 36.7	43 27 38.9	Dalan Dzadgad		W-E Gurvan-Saikhan fault	13	32
11m8-3	104 20 41.3	43 27 51.6	Dalan Dzadgad		W-E Gurvan-Saikhan fault	20	22
11m8-4a	104 22 35.1	43 27 42.2	Dalan Dzadgad		W-E Gurvan-Saikhan thrust	5	9
11m8-4b	104 22 35.1	43 27 42.2	Dalan Dzadgad		W-E Gurvan-Saikhan thrust	4	9
11m8-6	104 42 41.4	43 26 22.3	Dalan Dzadgad		W-E Tsetsei foreberg	6	10
11m9-1a	104 43 08.5	43 26 22.1	Dalan Dzadgad		W-E Tsetsei foreberg	14	45
11m9-1b	104 43 08.5	43 26 22.1	Dalan Dzadgad		W-E Tsetsei foreberg	16	45
11m9-2a	104 42 25.6	43 26 22.8	Dalan Dzadgad		W-E Tsetsei foreberg	5	13
11m9-2b	104 42 25.6	43 26 22.8	Dalan Dzadgad		W-E Tsetsei foreberg	4	13

N o t e. n – number of data used; nt – total number of measured data; σ_1, σ_2, σ_3 – stress axes; pl – plunge, az – azimuth; R – stress ratio; SH_{max} – horizontal maximum compressional axes; SH_{min} – horizontal minimum compressional axes; R′: stress regime index; F5 – misfit optimization function (http://www.damiendelvaux.be/Tensor/UserGuides/user-guides.html).

П р и м е ч а н и е. n – количество трещин, использованных для реконструкции; nt – общее количество трещин в наборе; σ_1, σ_2, σ_3 – главные оси напряжений; pl – угол погружения оси; az – азимут погружения оси; R – коэффициент стресс-тензора; SH_{max} – максимальное горизонтальное напряжение; SH_{min} – минимальное горизонтальное напряжение; R′ – индекс режима напряжений; F5 – функция оптимизации (http://www.damiendelvaux.be/Tensor/UserGuides/user-guides.html).

$\sigma_1$pl	$\sigma_1$az	$\sigma_2$pl	$\sigma_2$az	$\sigma_3$pl	$\sigma_3$az	R	SH_{max}	SH_{min}	R'	Stress Regime	Fct	Fct_Val
9	10	11	12	13	14	15	16	17	18	19	20	21
20	97	68	250	9	4	0.39	95	5	1.61	Pure STRIKE-SLIP	F5	4.7
78	42	12	236	3	145	0.68	55	145	0.68	Pure EXTENSIONAL	F5	9.2
1	1	2	271	88	125	0.53	1	91	2.53	Pure COMPRESSIONAL	F5	1.5
5	27	0	117	85	211	0.75	27	117	2.75	Pure COMPRESSIONAL	F5	7.5
2	178	1	268	88	36	0.6	177	87	2.6	Pure COMPRESSIONAL	F5	9.2
8	10	0	100	82	190	0.53	10	100	2.53	Pure COMPRESSIONAL	F5	2.1
7	185	2	275	82	22	0.45	4	94	2.45	Pure COMPRESSIONAL	F5	5
4	30	58	293	32	123	0.67	32	122	1.33	Pure STRIKE-SLIP	F5	5.9
2	180	12	270	78	82	0.05	180	90	2.05	Strike-slip COMPRESSIONAL	F5	2.2
10	137	6	46	78	285	0.57	138	48	2.57	Pure COMPRESSIONAL	F5	4.4
21	321	40	212	42	72	0.75	154	64	2.75	Oblique COMPRESSIVE	F5	8.2
19	227	70	28	6	135	0.5	45	135	1.5	Pure STRIKE-SLIP	F5	0.8
5	9	10	278	79	123	0.01	8	98	2.01	Strike-slip COMPRESSIONAL	F5	1.2
21	346	3	77	69	175	0.35	165	75	2.35	Pure COMPRESSIONAL	F5	2.8
13	240	77	68	2	331	0.75	60	150	1.25	Extensional STRIKE-SLIP	F5	4.6
13	189	65	309	21	94	0.59	6	96	1.41	Pure STRIKE-SLIP	F5	6.3
5	243	79	359	10	152	0.36	62	152	1.64	Pure STRIKE-SLIP	F5	4.6
2	5	8	95	82	263	0.29	4	94	2.29	Pure COMPRESSIONAL	F5	1.2
11	40	76	179	9	308	0.5	39	129	1.5	Pure STRIKE-SLIP	F5	4.4
6	66	8	335	80	192	0	65	155	2	Strike-slip COMPRESSIONAL	F5	6
14	201	62	83	24	297	0.16	21	111	1.84	Compressional STRIKE-SLIP	F5	2.8
30	350	26	244	49	120	0.64	11	101	2.64	Oblique COMPRESSIVE	F5	10.2
6	181	73	71	16	273	0.41	2	92	1.59	Pure STRIKE-SLIP	F5	5.1
1	63	37	154	53	331	0.12	62	152	2.12	Strike-slip COMPRESSIONAL	F5	2.5
12	60	36	321	51	166	0.04	60	150	2.04	Strike-slip COMPRESSIONAL	F5	5.7
5	203	24	111	65	305	0.15	23	113	2.15	Strike-slip COMPRESSIONAL	F5	6.6
17	60	25	322	59	181	0.41	65	155	2.41	Pure COMPRESSIONAL	F5	5.4
7	357	0	87	83	180	0.59	177	87	2.59	Pure COMPRESSIONAL	F5	5.9
1	82	63	350	27	173	0.04	82	172	1.96	Compressional STRIKE-SLIP	F5	0.6
14	250	2	160	76	61	0.63	71	161	2.63	Pure COMPRESSIONAL	F5	7.3
6	58	81	193	6	327	0.6	57	147	1.4	Pure STRIKE-SLIP	F5	3.8
30	204	53	345	19	103	0.66	16	106	1.34	Pure STRIKE-SLIP	F5	8.9
25	31	41	277	39	143	0.26	34	124	1.74	Oblique COMPRESSIVE	F5	4.9
12	186	3	277	78	19	0.5	5	95	2.5	Pure COMPRESSIONAL	F5	5
11	251	74	119	11	343	0.33	71	161	1.67	Pure STRIKE-SLIP	F5	5.2
0	230	11	140	79	322	0.34	49	139	2.34	Pure COMPRESSIONAL	F5	9.3
31	84	56	291	13	182	0.33	86	176	1.67	Pure STRIKE-SLIP	F5	2.6
18	237	19	333	63	106	0.03	56	146	2.03	Strike-slip COMPRESSIONAL	F5	2.4
5	62	76	312	13	153	0.6	62	152	1.4	Pure STRIKE-SLIP	F5	6.4
6	20	38	115	51	282	0.38	18	108	2.38	Pure COMPRESSIONAL	F5	1.6
1	20	11	110	79	283	0.7	20	110	2.7	Pure COMPRESSIONAL	F5	5
1	252	61	343	29	161	0.33	71	161	1.67	Pure STRIKE-SLIP	F5	2.4
3	186	3	276	86	47	0.76	5	95	2.76	Radial COMPRESSIONAL	F5	6.1
15	273	64	37	20	177	0.49	89	179	1.51	Pure STRIKE-SLIP	F5	2.5
1	174	2	84	88	285	0.5	174	84	2.5	Pure COMPRESSIONAL	F5	6
13	11	1	281	77	189	0.69	11	101	2.69	Pure COMPRESSIONAL	F5	6.8
36	237	52	79	11	335	0.64	62	152	1.36	Pure STRIKE-SLIP	F5	5.2
20	248	27	348	55	127	0.48	60	150	2.48	Pure COMPRESSIONAL	F5	7.5
25	55	53	184	25	313	0.3	51	141	1.7	Pure STRIKE-SLIP	F5	0.9

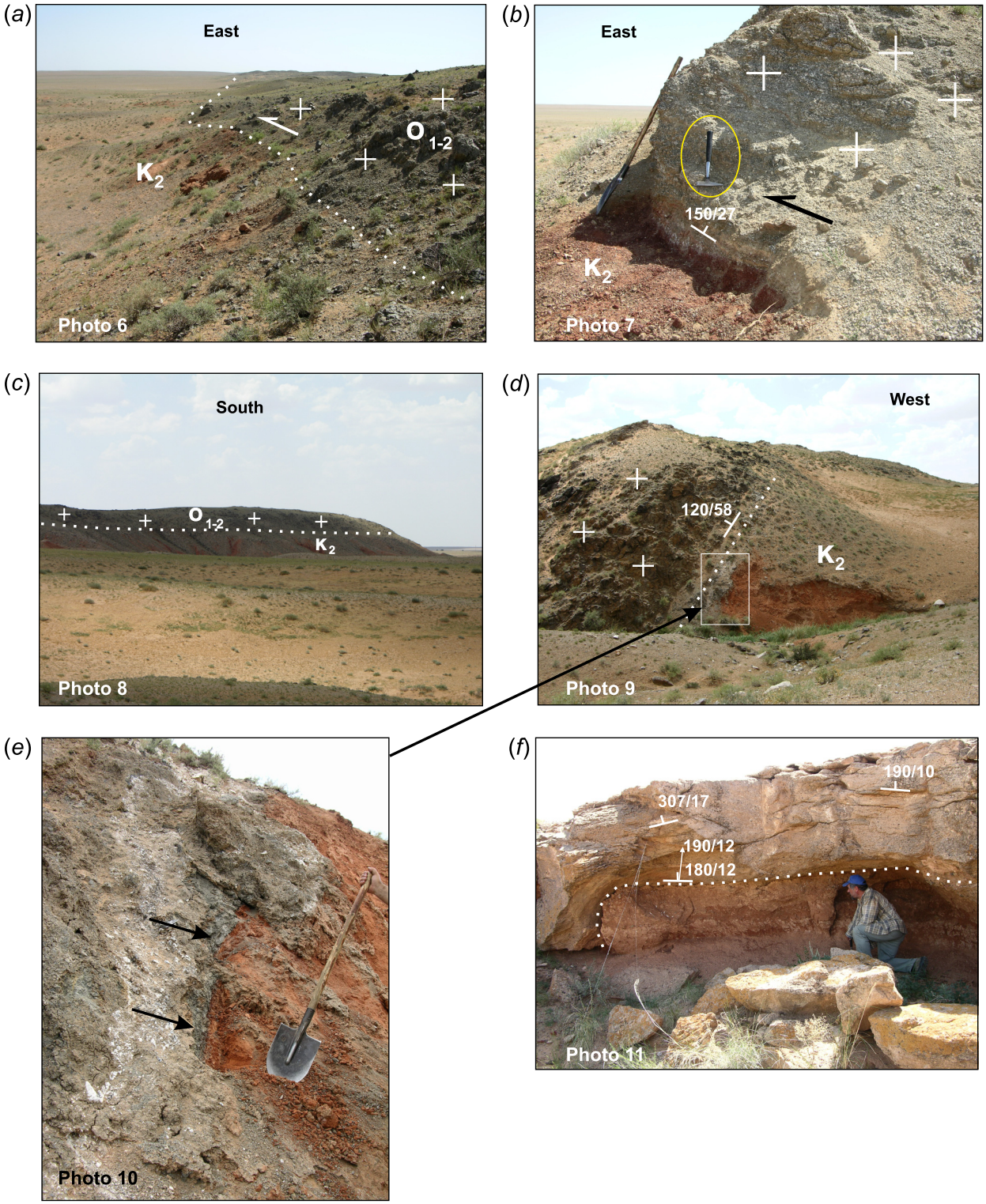

Fig. 8. Cenozoic deformation near the southern fault bordering the Dalain–Khunda basin (southwest of Erdene Somon): (*a*) – thrust of the crystalline basement rocks onto the Upper Cretaceous sediments, (*b*) – thrust contact zone, (*c*) – view of the scarp in the north, (*d*) – reverse-type displacement of the crystalline basement rocks onto the Upper Cretaceous sediments, (*e*) – reverse fault with the weathering gouge zone, (*f*) – along the layer detachmentin the Upper Cretaceous red sediments with crushed and mixed rocks (east of Erdene Somon). See the locations in Fig. 5 and 10.

Рис. 8. Кайнозойские деформации в зоне южного бортового разлома Далайн-Хундийской впадины (к юго-западу от сомона Эрдэнэ): (*a*) – надвиг пород кристаллического основания на верхнемеловые отложения, (*b*) – зона надвигового контакта, (*c*) – вид на уступ с севера, (*d*) – взброс пород кристаллического основания на верхнемеловые отложения, (*e*) – зона взбросового контакта с линейной корой выветривания, (*f*) – послойные срывы с раздробленной и закатанной между слоями массой пород в верхнемеловых отложениях (к востоку от сомона Эрдэнэ). Местоположение фото показано на рис. 5 и 10.

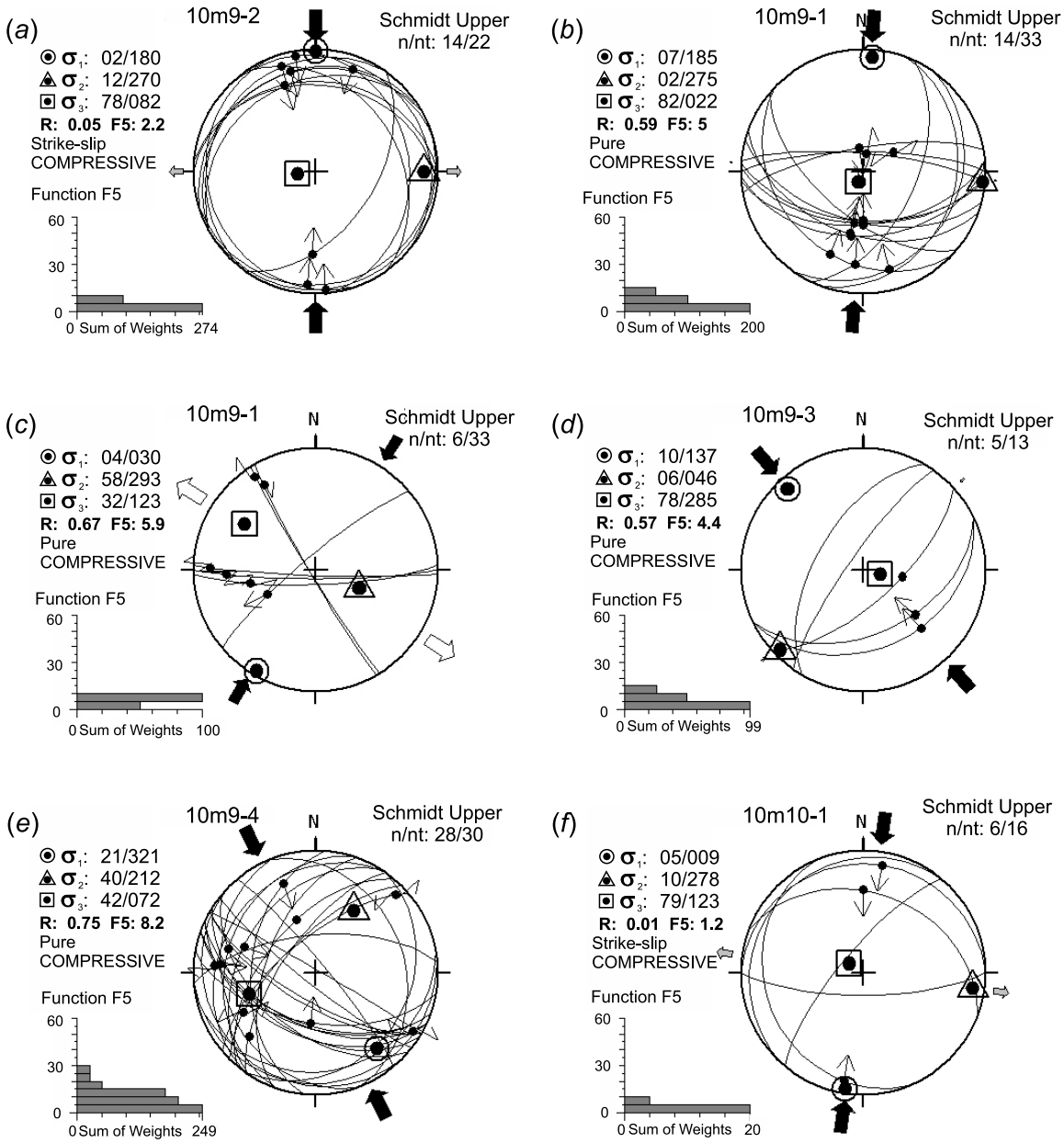

Fig. 9. Paleostress reconstructions for fault zones in the Dalain-Khunda basin. Numbers of stress tensors correspond to the numbers of observation points in Fig. 5 and Fig. 10.

Рис. 9. Реконструкции палеонапряжений в зонах разломов Далайн-Хундийской впадины. Номер стресс-тензора соответствует номеру точки наблюдения на рис. 5 и рис. 10.

The stress field reconstructions for the Paleozoic rock outcrops along the scarp show strike-slip, compression and transpression regimes with the NE-trending axis of compression (Fig. 18, *f*, *g*, *h*; Fig. 19, *a*, *b*, *c*; see Table).

The W-E-trending Tsetsei uplift located east of the Gurvan-Saikhan uplift is syndepositional in relation to the Mesozoic basins in this region [*Yanshin, 1975*] (see Fig. 4, *c*). Its southern side was activated in the Cenozoic as evidenced by clear fault scarps bordering some ranges in the south, as well as the forebergs that 'cut' the northern side of the Argalint basin. Near the Khan-Ula mountain, the southern side of the basic rock block is overlain by the Cenozoic (50 Ma) basalts and displaced by the two W-E-striking left-lateral strike-slip faults (Fig. 16, *c*).The offset is about 60 m along the northern fault branch and 250 m along the southern fault branch. The northern block is raised relative to the southern one, which indicates a reverse component of displacement along the fault. Left-lateral horizontal displacement with reverse component where found along southern boundary of the small W-E-trending ridge-forberg located at a distance of 6.0 km south (Fig. 16, *d*).The scarp is 3.0 to 4.0 m high. The tempo-

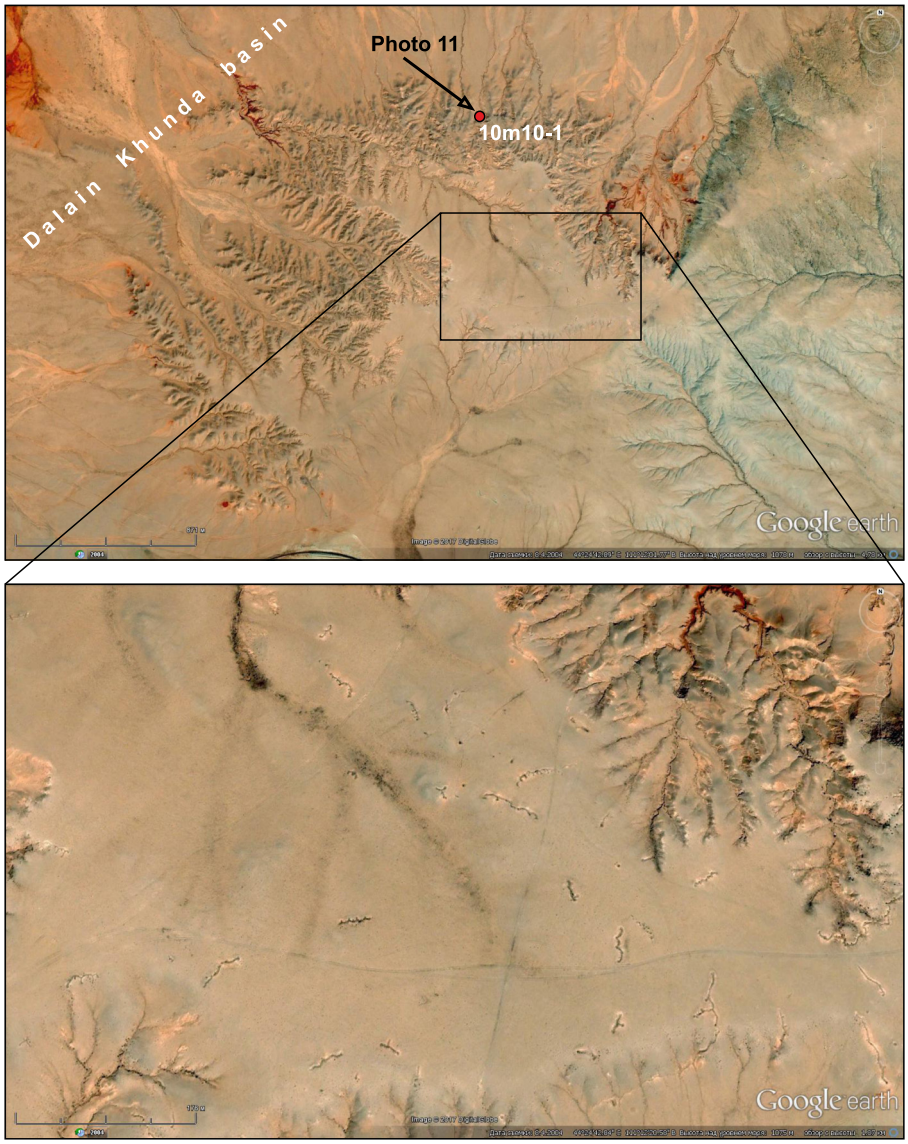

Fig. 10. Fragments of Spot (Google Earth) satellite images showing the erosional pattern near the southern fault bordering the Dalain-Khunda basin (east of Erdene Somon).

Рис. 10. Фрагменты космических снимков «Spot» (Google Earth), показывающие формирование эрозионной сети в зоне южного бортового разлома Далайн-Хундийской впадины к востоку от сомона Эрдэнэ.

rary water stream valleys are shifted, and the left-lateral strike-slip component amounts are to 6.0–7.0 m (Fig. 17, *d*). The stress field reconstructions for this fault zone show compression and strike-slip regimes with the NE-trending and N-S axes of compression (Fig. 19, *d* to *h*; see Table).

5. Discussion

Comparing the data on the geological development of the East and South Gobi depressions suggests a similar history of the evolution of these two neighbouring areas in the Late Jurassic – Early Cretaceous (rifting) and Late Cretaceous – Paleogene (tectonic quiescence). Later on, in the Cenozoic, the depressions were activeted in completely different modes.

In the Cenozoic, the East Gobi depression was in tectonic quiescence in the Late Cretaceous – Paleogene [*Yanshin, 1975*], on the one side. On the other side, there is evidence of the active left-lateral strike-slip displacements along in the East Gobi fault zone (EGFZ) in the Tertiary period [*Graham et al., 2001; Johnson, 2004; Webb, Johnson, 2006; Yue, Liou, 1999*]. According to [*Johnson, 2004; Webb, Johnson, 2006*], EGFZ displaced both the synrift Late Jurassic – Early Cretaceous sediments of the Dzunbai and Unegt basins and the unconformable surface between the Lower and Upper Cretaceous sediments. Besides, it displaced and deformed the overlying Upper Cretaceous – Cenozoic sediments.

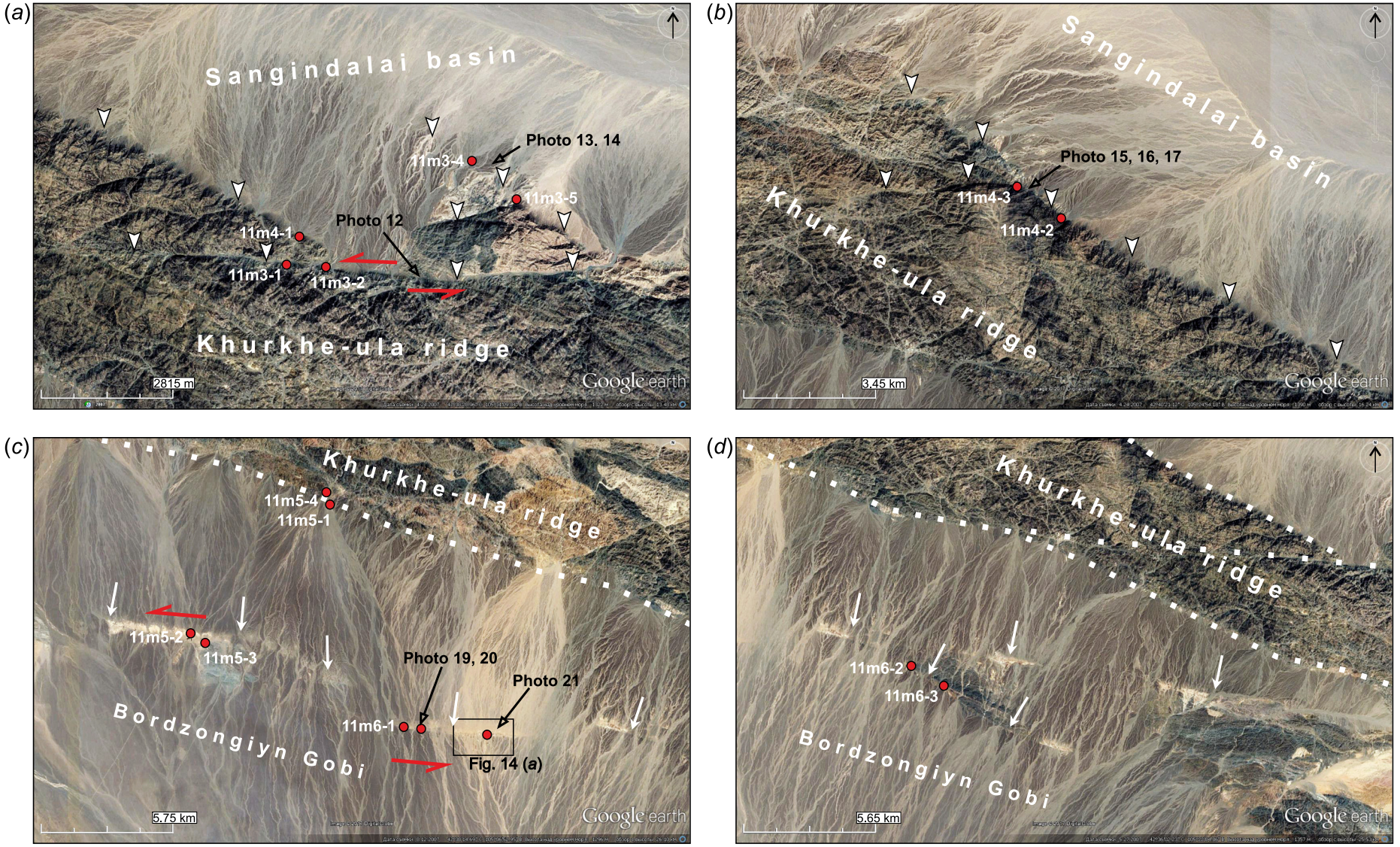

Fig. 11. Fragments of Spot (Google Earth) satellite images showing active faults in the Khurkhe-Ula uplift (South Gobi depression, eastern-most termination of Gobi Altai). Locations of (*a*), (*b*), (*c*), and (*d*) images are shown in Fig. 4 (*b*). Observation points are marked by red circles and corresponding code numbers.

Рис. 11. Фрагменты космических снимков «Spot» (Google Earth), показывающие активные разломы поднятия Хурхэ-Ула (Южногобийская впадина, крайнее восточное окончание Гобийского Алтая). Положение рисунков (*a*), (*b*), (*c*), (*d*) показано на рис. 4 (*b*). Красными точками обозначены точки наблюдения с соответствующим кодовым номером.

Geodynamics & Tectonophysics 2018 Volume 9 Issue 3 Pages 855–888

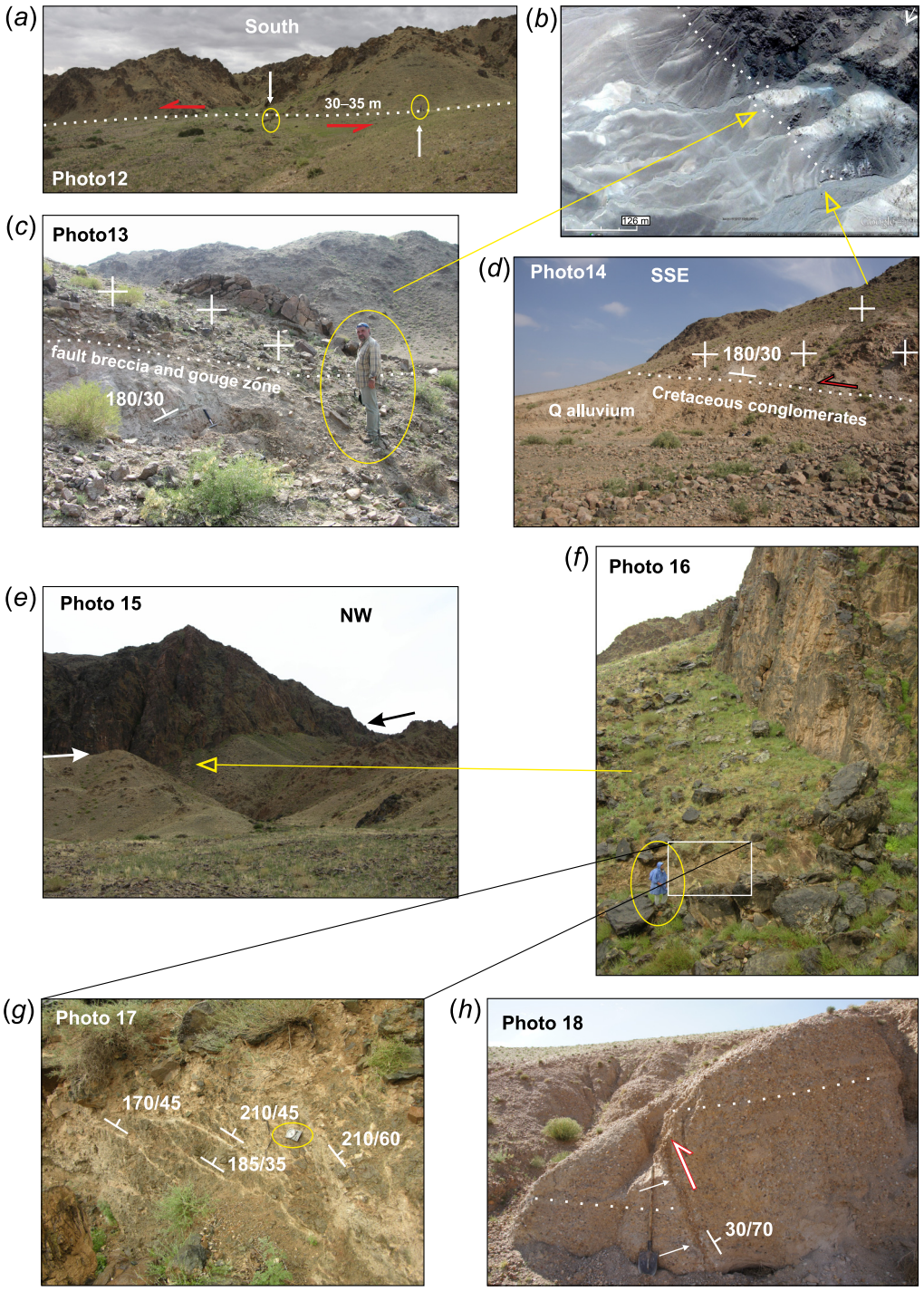

Fig. 12. Late Cenozoic deformation in active fault zones in the northeastern side of the Khurkhe-Ula uplift. (*a*) – left-lateral strike-slip along the W-E fault; (*b*) – fragments of Spot (Google Earth) satellite images near the Mogoin-Khuduk site; (*c*) – weathering gouge zone at the thrust contact; (*d*) – thrust of the crystalline basement rocks onto the loose Mesozoic conglomerates; (*e*) – view of the NW-trending scarp from the east in the northeastern side of the Khurkhe–Ula uplift; (*f*), (*g*) – crushed rock zone at the base of the NW-trending scarp; (*h*) – deformation of poorly cemented conglomerates in the southwestern side of the Sangiyndalai basin. See the locations in Fig. 11, (*a*), (*b*).

Рис. 12. Деформации в зонах активных разломов северо-восточного борта поднятия Хурхэ-Ула. (*a*) – левосторонний сдвиг по субширотному разлому, (*b*) – фрагмент космического снимка «Spot» (Google Earth) окрестности точки наблюдения Могойн-Худук, (*c*) – линейная кора выветривания в зоне надвигового контакта, (*d*) – надвиг пород кристаллического основания на рыхлые мезозойские конгломераты, (*e*) – вид с востока на уступ северо-западного простирания в северо-восточном борту поднятия Хурхэ-Ула, (*f*), (*g*) – зона дробления и катаклаза в основании уступа северо-западного простирания, (*h*) –деформации в слабосцементированных конгломератах юго-западного борта Сангийндалайской впадины. Местоположение фото показано на рис. 11, (*a*), (*b*).

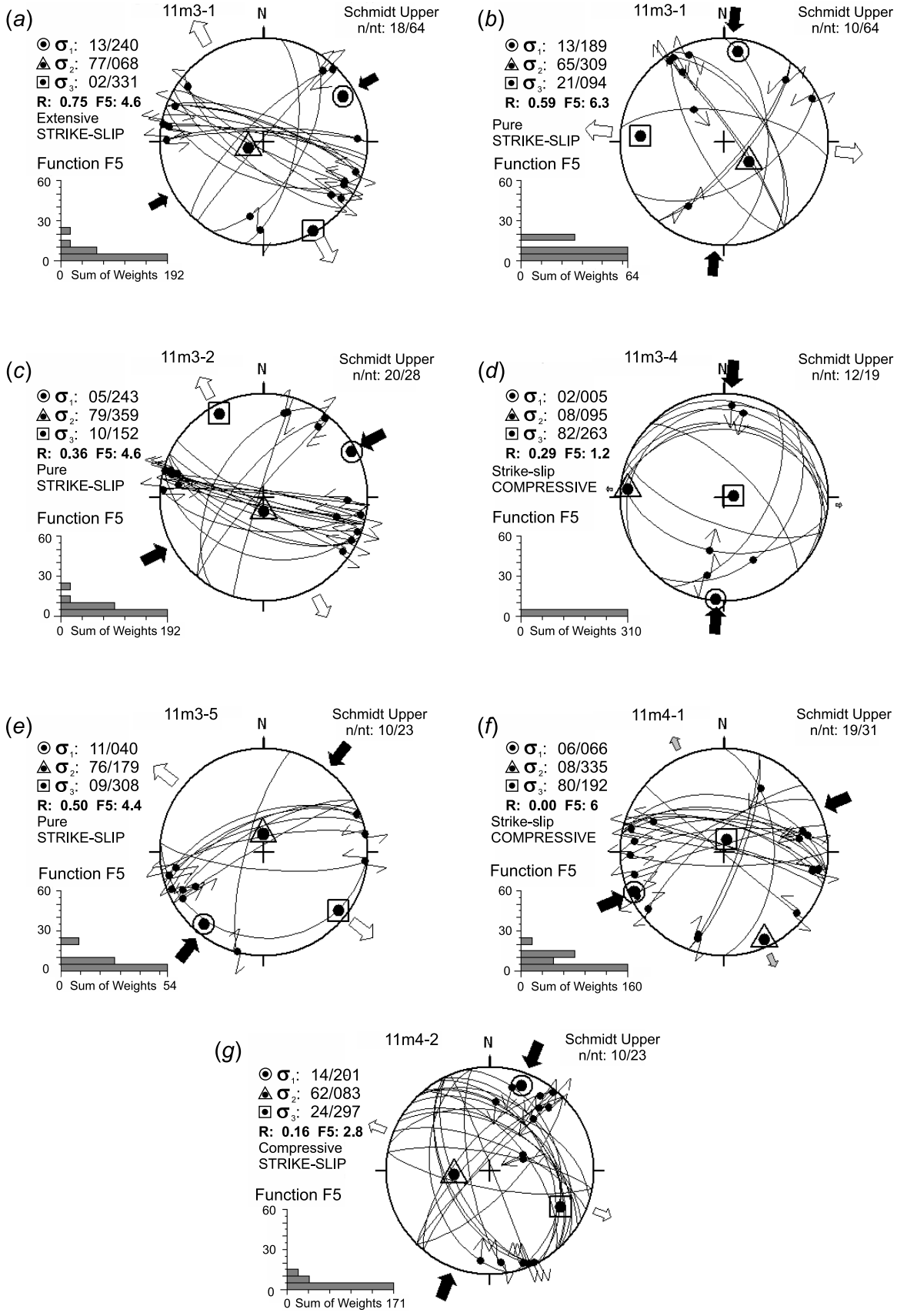

Fig. 13. Paleostress reconstructions for active fault zones in the northeastern slope of the Khurkhe-Ula uplift. Numbers of stress tensors correspond to the numbers of observation points in Fig. 11, (*a*), (*b*).

Рис. 13. Реконструкции палеонапряжений в зонах активных разломов северо-восточного склона поднятия Хурхэ-Ула. Номер стресс-тензора соответствует номеру точки наблюдения на рис. 11, (*a*), (*b*).

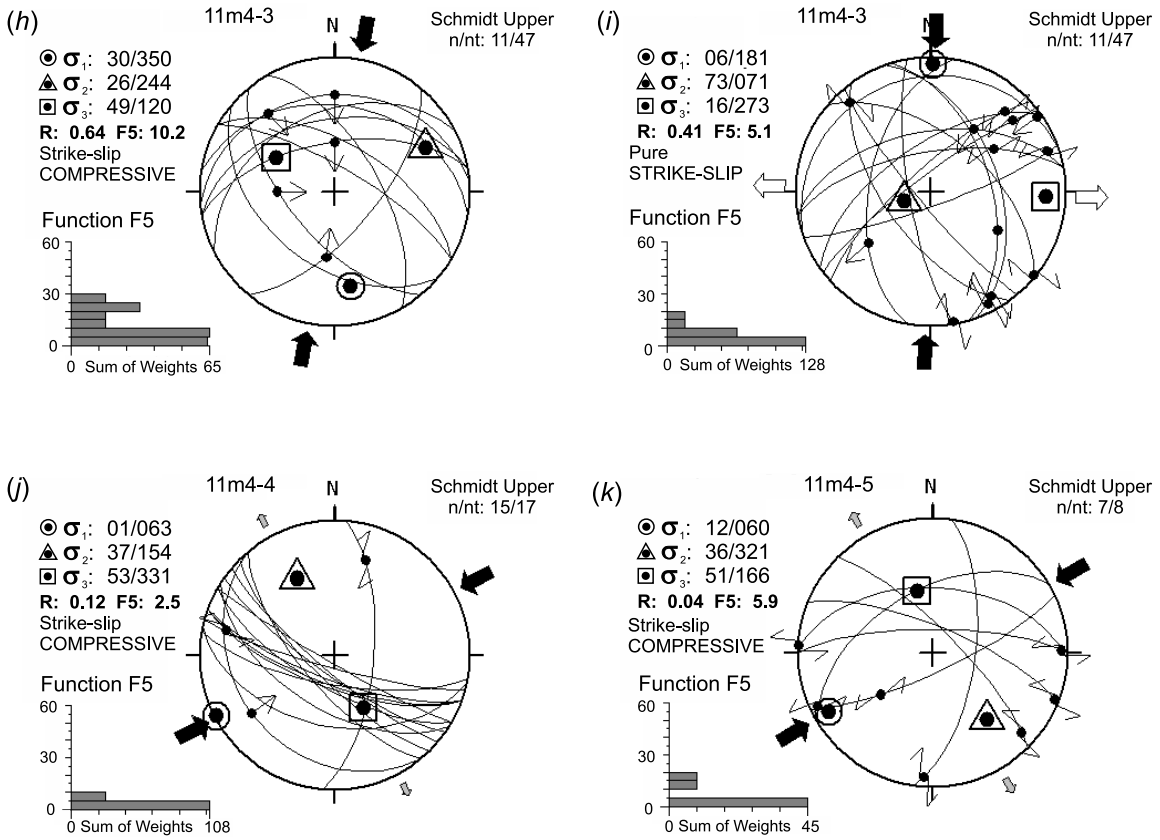

Fig. 13 (end)

Рис. 13 (окончание)

The strike-slip kinematics of displacements along the fault zone is evidenced by the contrasting sediment formations across the fault strike [*Johnson, 2004*] and the stress field reconstructions showing strike-slip regime in the Tsagan Subarga uplift (Tsagan-Suburga, Tavan-Khar, Ulgei-Khid ridges) [*Webb, Johnson, 2006*]. The axes of compression and extension trend in the NNW and ENE directions, respectively (see the stress tensors marked in grey in Fig. 20). In [*Webb, Johnson, 2006*], the strike-slip amplitude is estimated at 100–150 km by displacement of Low Cretaceous markers and dated Cenozoic, similar to [*Darby et al., 2005*]. According to [*Darby et al., 2005; Yue, Liou, 1999*], it is assumed a kinematic relation between EGFZ and the Altyn Tagh fault through the system of left-lateral strike-slip faults in the Alxa region located north and northeast of Tibet. According to [*Yue, Liou, 1999*], the EGFZ, the Altyn Tagh and Alxa faults had developed as a single fault system since the Oligocene. The system ceased its activity 13–16 Ma ago as the left-lateral strike-slip displacements along the Altyn Tagh fault were transfered to thrusting, crustal shortening and uplifting in the Qilian Shan region. The Early Cenozoic displacement along EGFZ is estimated by [*Yue, Liou, 1999*] as about 400 km. According to [*Darby et al., 2005*], strike-slip faulting developed in the Alxa region in two stages. In the post Cretaceous – pre-Middle Miocene stage, large amplitude left-lateral strike-slip displacements took place along the Altyn Tagh fault and the system of the Alxa left-lateral strike-slip faults (i.e. the NE-trending continuation of Altyn Tagh fault). Further to NE, left-lateral strike-slip displacements where either transferred to EGFZ or transformed into normal faulting in the Periordos rift system. The Upper Cretaceous markers show the offset amplitudes of 70–150 km [*Darby et al., 2005*]. In the post Miocene – recent stage, there are the left-lateral strike-slip faults of limited amplitudes (less than 3.0 km) in the Alxa region and lower rates of strike-slip displacements along the Altyn Tagh fault as the left-lateral strike-slip in the Altyn Tagh fault was accommodated by thrusting in the Qilian Shan region. According to [*Webb, Johnson, 2006*], the redistribution of deformation in the NE periphery of the Indo-Asian collision zone correlates with changes in the boundary conditions at another interplate boundary, specifically the replacement of transtension with transpression in the NE segment of the Western Pacific interplate boundary in the Late Miocene [*Worrall et al., 1996*]. This may also be a cause of EGFZ inactivity since the Late Miocene.

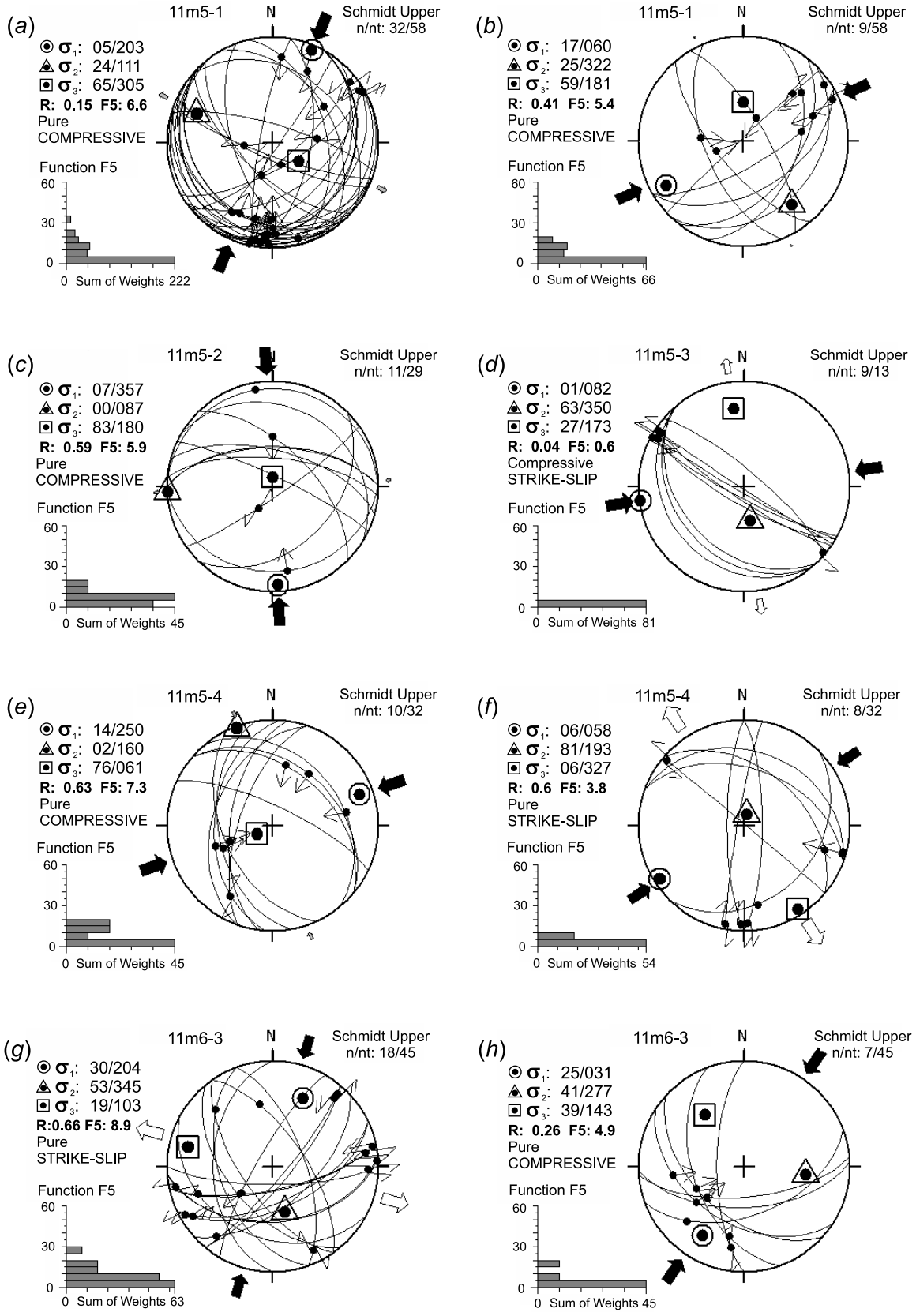

Fig. 14. Paleostress reconstructions for active fault zones in the northwestern slope of the Khurkhe-Ula uplift and the northwestern side of the Gunkhuduk basin (Bordzongiyn Gobi site). The numbers of stress tensors correspond to the numbers of observation points in Fig. 11, (*c*), (*d*).

Рис. 14. Реконструкции палеонапряжений в зонах активных разломов юго-западного склона поднятия Хурхэ-Ула и северо-западного борта Гунхудукской впадины (урочище Бордзонгийн-Гоби). Номер стресс-тензора соответствует номеру точки наблюдения на рис. 11, (*c*), (*d*).

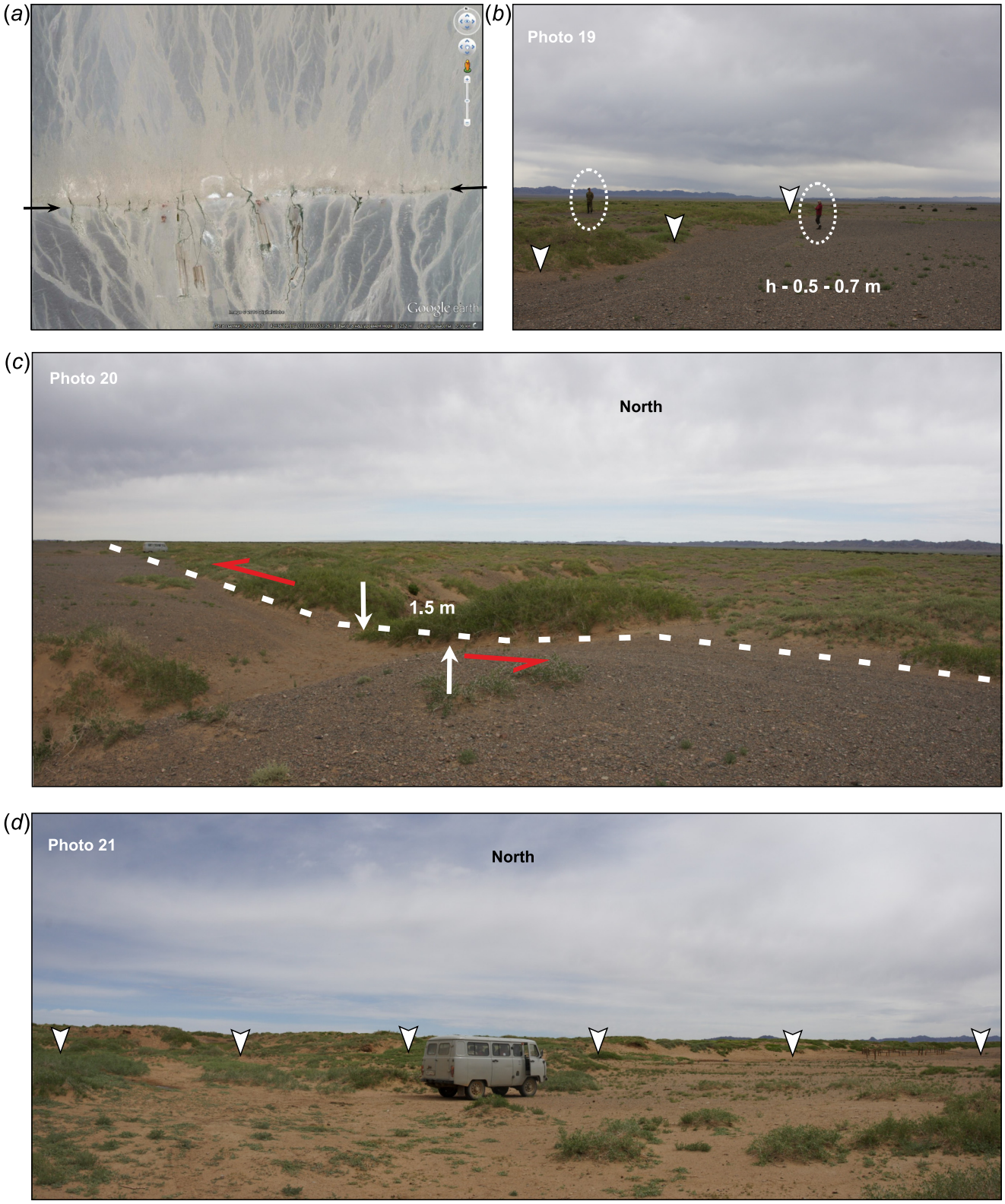

Fig. 15. Late Cenozoic deformation in active fault zones in the northwestern side of the Gunkhuduk basin (Bordzongiyn Gobi site). (*a*) – fragment of theSpot (Google Earth) image of one of the W-E scarps across the low-angle plain (the location is shown in Fig. 11 (*c*)), (*b*) – W-E scarp, (*c*) – left-lateral strike-slip of the temporary stream valley, (*d*) – view of one of the W-E scarps from the south. See the locations in Fig. 11 (*c*), (*d*).

Рис. 15. Деформации в зонах активных разломов северо-западного борта Гунхудукской впадины (урочище Бордзонгийн-Гоби): (*a*) – фрагмент космического снимка «Spot» (Google Earth) одного из субширотных уступов, пересекающих наклонную равнину бэль (положение рисунка показано на рис. 11, (*c*)), (*b*) – уступ субширотного простирания, (*c*) – левосторонний сдвиг долины временного водотока, (*d*) – вид на один из субширотных уступов с юга. Местоположение фото показано на рис. 11, (*c*), (*d*).

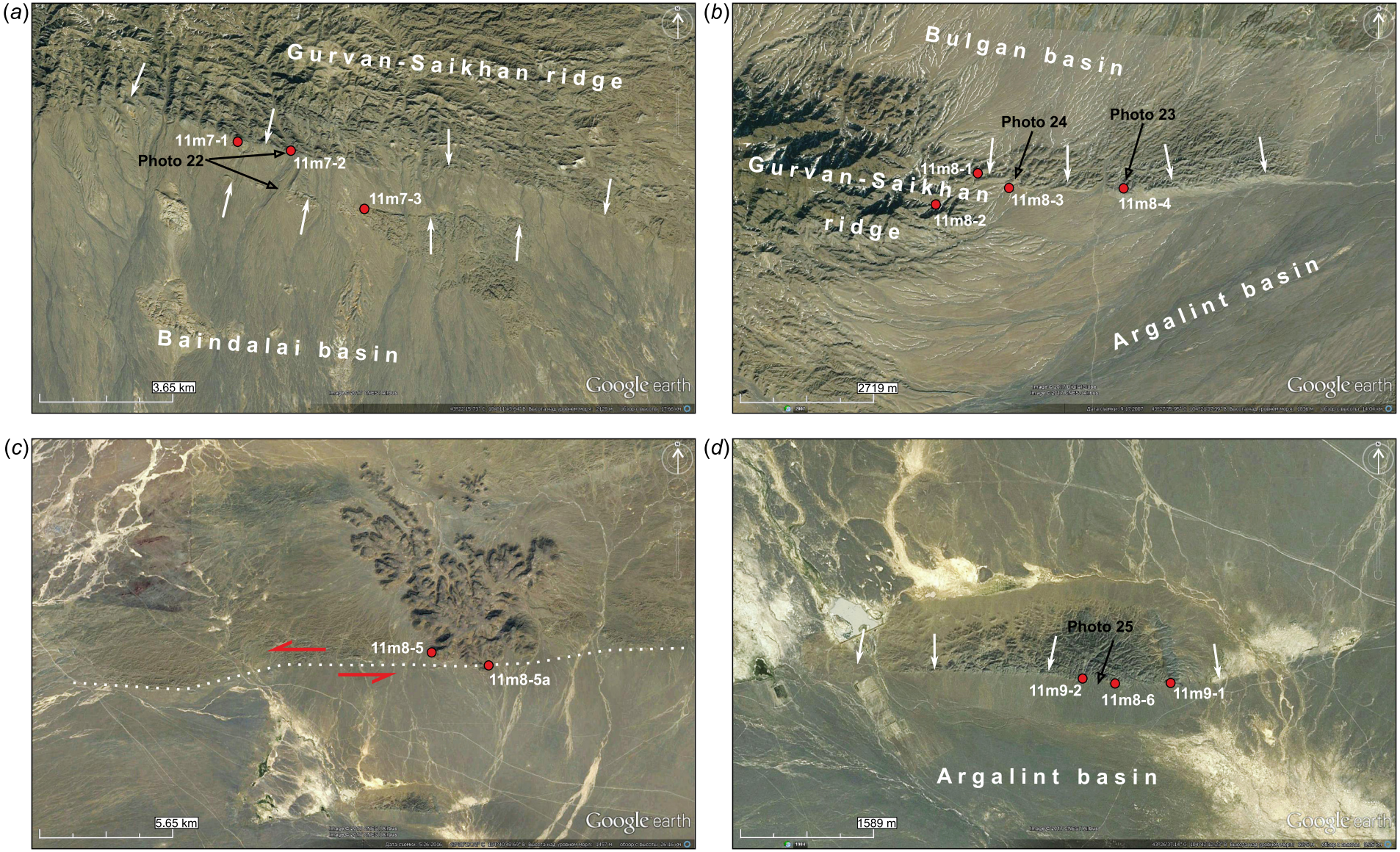

Fig. 16. Fragments of Spot (Google Earth) satellite images showing active faults in the Gurvan-Saikhan and Tsetsei uplifts. Locations of Fig. 16 (*a*), (*b*), (*c*), (*d*) are shown in Fig. 4, (*c*). Observation points are marked by red circles.

Рис. 16. Фрагменты космических снимков «Spot» (Google Earth), показывающих активные разломы поднятия Гуван-Сайхан и Цэцэйского поднятия. Положение рис. 16 (*a*), (*b*), (*c*), (*d*) показано на рис. 4 (*c*). Красными точками обозначены пункты наблюдения.

Geodynamics & Tectonophysics 2018 Volume 9 Issue 3 Pages 855–888

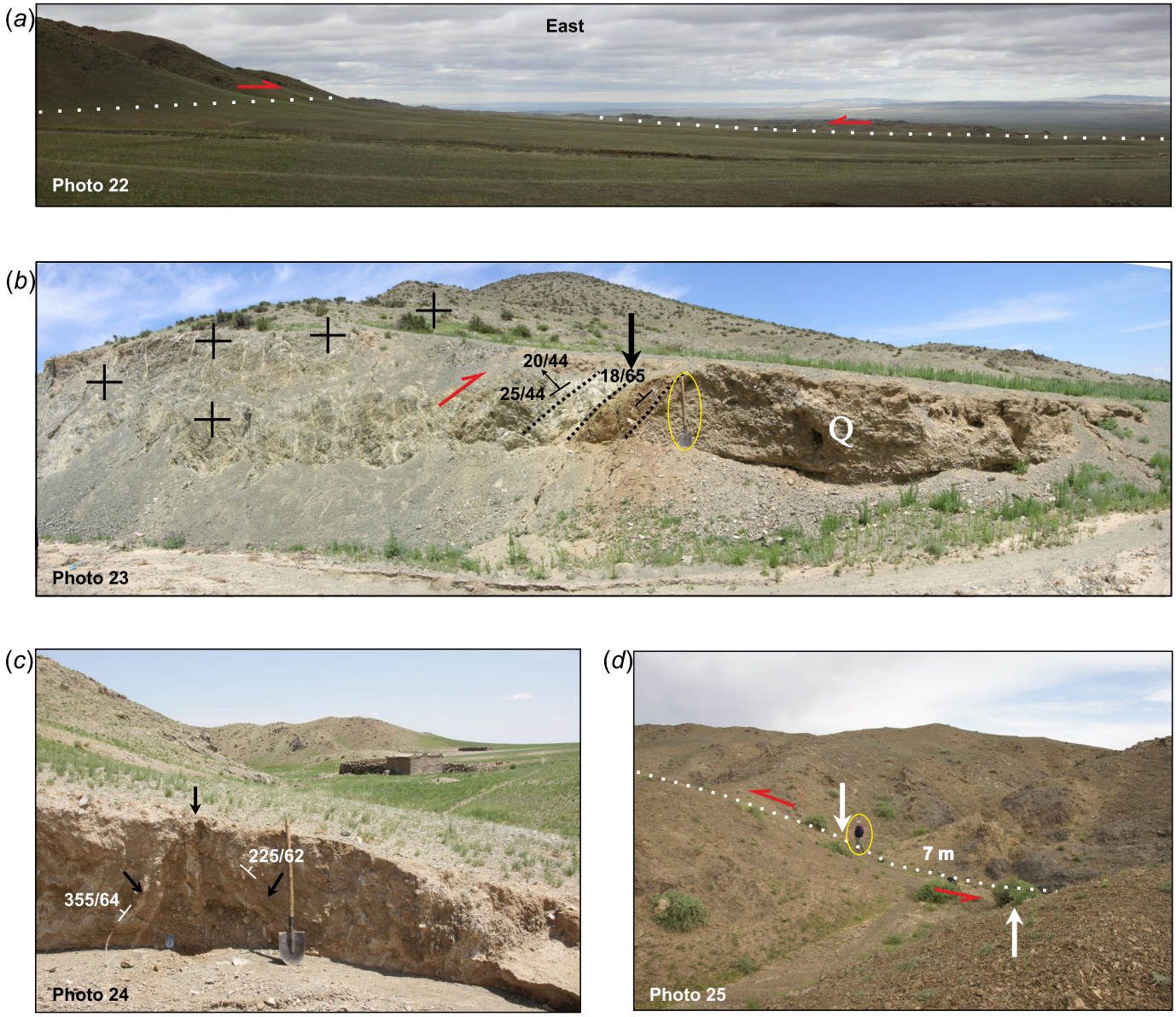

Fig. 17. Late Cenozoic deformation in active fault zones of the Gurvan-Saikhan and Tsetsei uplifts. (*a*) – view of the southern fault scarp bordering the Gurvan-Saikhan uplift near Khurmen Somon, (*b*) – thrust of the mylonitized bedrocks onto the Quaternary deluvium sediments of the slope, (*c*) – deformation of deluvium sediments near the W-E fault (eastern termination of the Gurvan-Saikhan uplift), (*d*) – left-lateral strike-slip of the temporary stream valley along the W-E fault zone in the southern side of one of the forbergs (Tsetsei uplift). See the locations in Fig. 16.

Рис. 17. Деформации в зонах активных разломов поднятия Гуван-Сайхан и Цэцэйского поднятия: (*a*) – вид на уступ южного бортового разлома поднятия Гурван-Сайхан вблизи сомона Хурмен, (*b*) – надвиг раздробленных милонитизированных коренных пород на склоновые четвертичные отложения, (*c*) – деформации склоновых отложений в зоне субширотного разлома (восточное окончание поднятия Гурван-Сайхан), (*d*) – левосторонний сдвиг долины временного водотока по зоне субширотного разлома в южном борту одного их форбергов Цэцэйского поднятия. Местоположение фото показано на рис. 16.

The post-Late Cretaceous thrusts observed in our study of the NE-trending scarps in the northern side of the Totoshan uplift (east of the EGFZ), the stress field reconstructions of compression and transpression regimes (Fig. 20) indicate that the N-S and NW compression was also active at the beginning of the Cenozoic. According to [*Tomurtogoo, 1999*], the faults bordering the SW part of the Dalain-Khunda basin control the spread of the Cenozoic (Paleogene) sedimentation. The most probable age of the deformation is thus Paleogene.

In time, a possible upper boundary for the above-mentioned compression may be the activity of the NE-trending structures in the Dariganga volcanic plateau

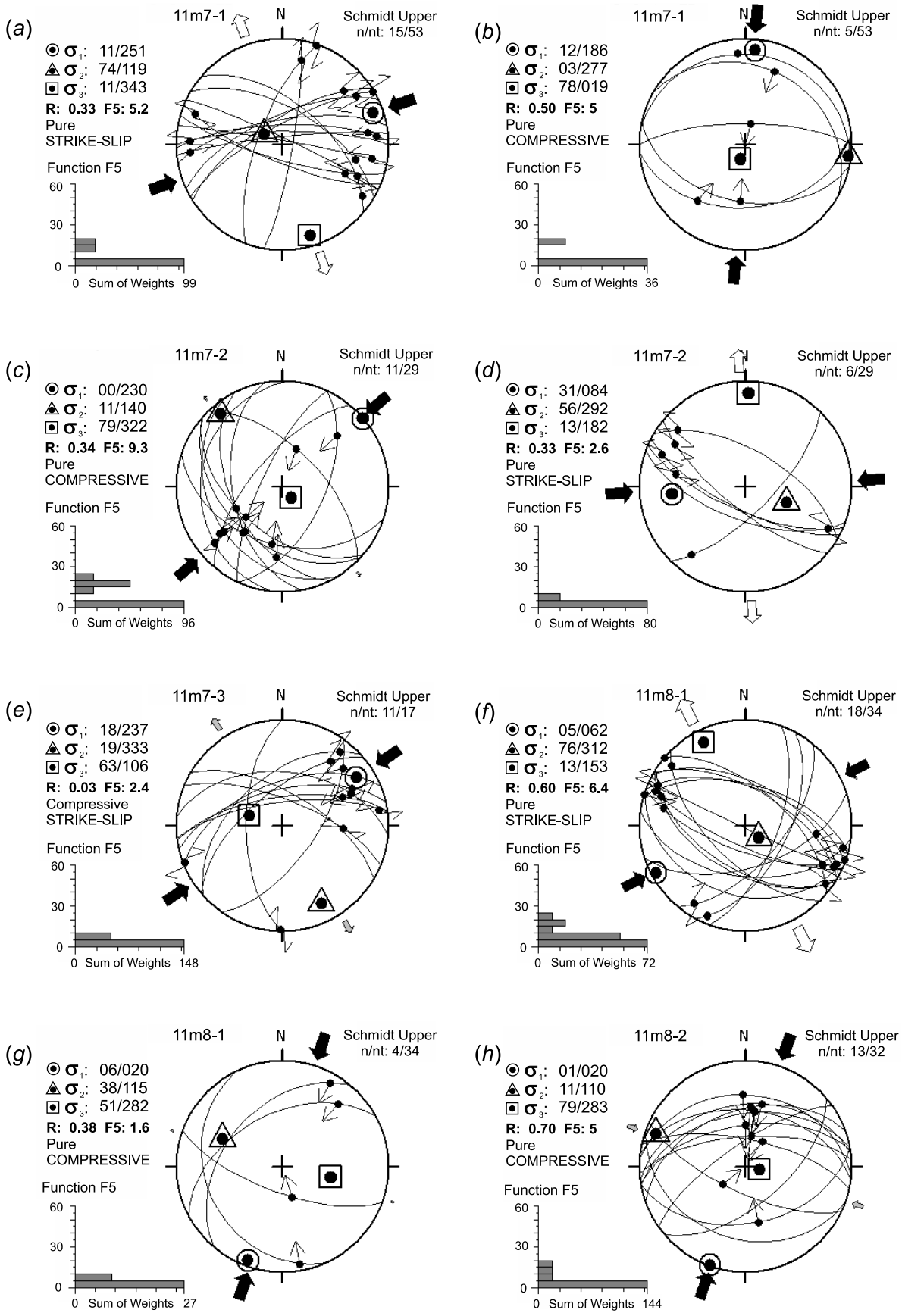

Fig. 18. Paleostress reconstructions for active fault zones of the Gurvan-Saikhan uplift. Numbers of stress tensors correspond to the numbers of observation points in Fig. 16.

Рис. 18. Реконструкции палеонапряжений в зонах активных разломов поднятия Гуван-Сайхан. Номер стресс-тензора соответствует номеру точки наблюдения на рис. 16.

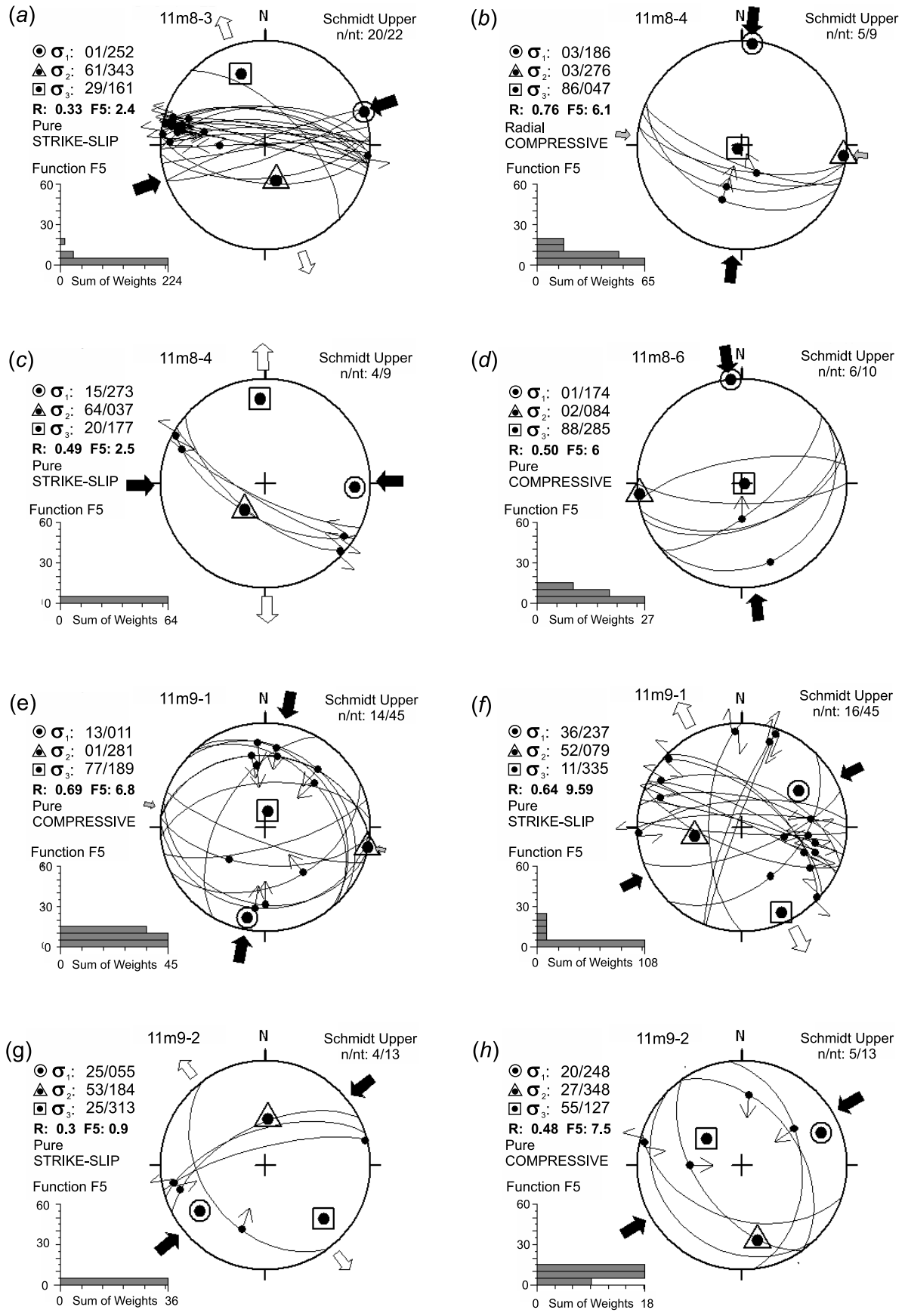

Fig. 19. Paleostress reconstructions for active fault zones of the Gurvan-Saikhan and Tsetsei uplifts. Numbers of stress tensors correspond to the numbers of observation points in Fig. 16.

Рис. 19. Реконструкции палеонапряжений в зонах активных разломов поднятия Гуван-Сайхан и Цэцэйского поднятия. Номер стресс-тензора соответствует номеру точки наблюдения на рис.16.

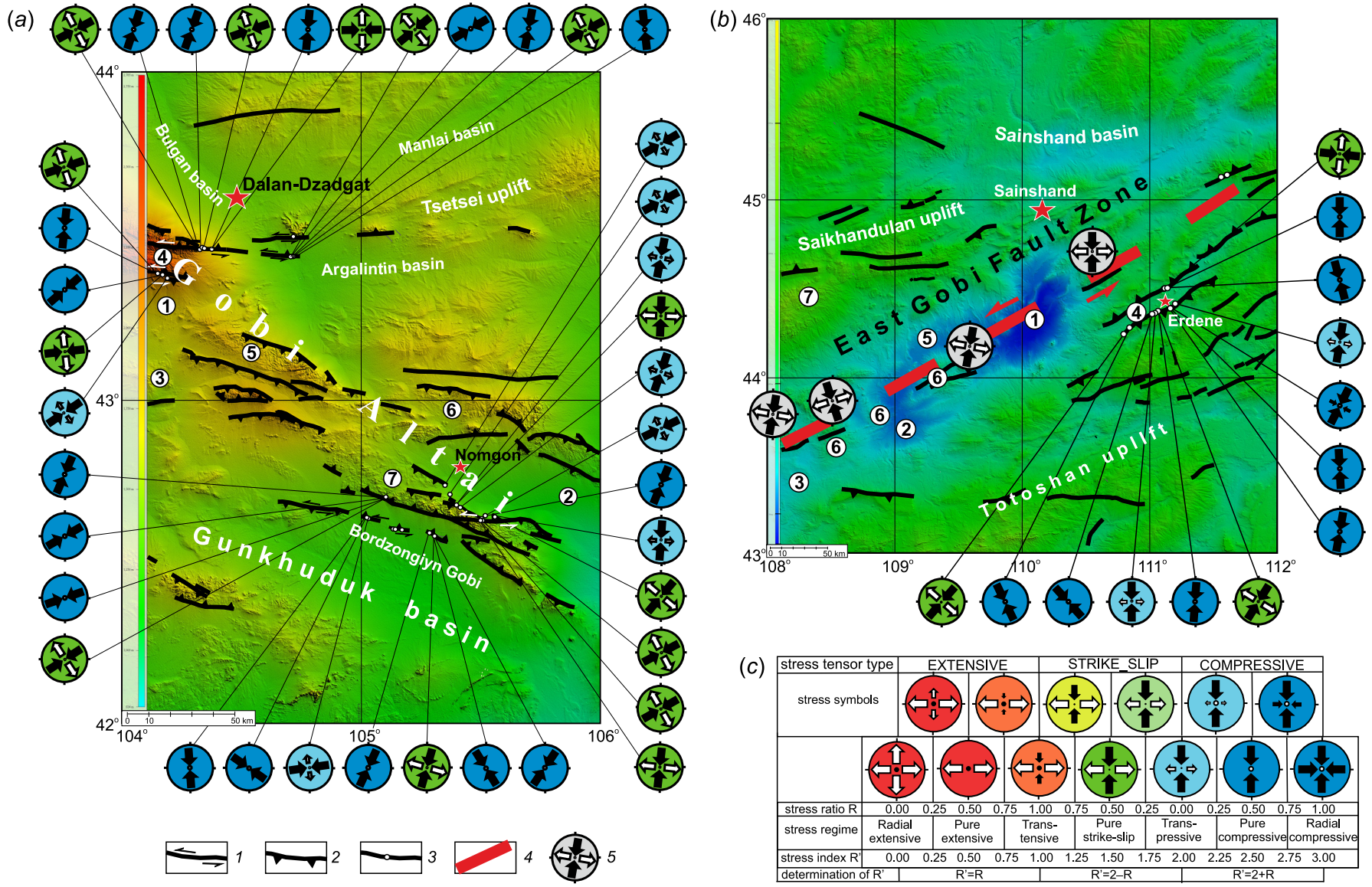

Fig. 20. Stress tensors for South Gobi (*a*) and East Gobi (*b*) depressions, and stress tensor classification by [*Delvaux et al., 1997*] (*c*).

1 – strike-slip faults; *2* – thrusts; *3* – observation points; *4* – East Gobi fault zone; *5* – paleostress reconstruction by [*Webb, Johnson, 2006*].

Рис. 20. Схема стресс-тензоров поля напряжений Южно-Гобийской (*a*) и Восточно-Гобийской (*b*) депрессий и классификация стресс-тензоров по [*Delvaux et al., 1997*] (*c*).

1 – сдвиги, *2* – надвиги, *3* – точки наблюдений, *4* – Восточно-Гобийская разломная зона, *5* – реконструкции поля напряжений по [*Webb, Johnson, 2006*].

Geodynamics & Tectonophysics 2018 Volume 9 Issue 3 Pages 855–888

located further to NE, which commenced in the Miocene under NW extension and continued until the Pleistocene. The magma flows were controlled by the NE- and, more rarely, W-E-striking faults, as evidenced by the chains of volcanic structures and basalt dikes. The activity in this region coincided in time with active extension in the Baikal rift and the formation of the Inchuan-Hetao rift zone in the Periordos rift system, which many authors relate to the Indo-Asian collision. The current tectonic activity in the Dariganga plateau is weak.

The NW compression source is still unknown, but possible causes for its occurrence are suggested in the literature. Firstly, local thrusting in the southeastern wing of EGFZ may be related to large-amplitude left-lateral strike-slip displacements along EGFZ in the Oligocene – Miocene. The Indo-Asian collision may be the source of the left-lateral strike-slip movements in this region. In this case, an explanation can be provided for the absence of similar deformation in the South Gobi depression, but the kinematic relation between the NE-trending thrusts and EGFZ still remains unclear. Secondly, there is evidence of the NW compression in North China in the post-Cretaceous period, which is driven by the Pacific subduction zone. According to [*Feng et al., 2010*], the movements of the Pacific plate were rearranged about 65 Ma ago and caused an inversion in the development of the Songliao basin, uplifting, folding and thrusting. According to [*Zhang et al., 2018*], the NNE trusting and folding occurred in a more southern region (Hanghua basin) and in an earlier period (Late Cretaceous). The long-distance action of plate interactions and the transfer of deformations into the lithospheric plate interior depend on the type of interaction. The most effective in this sense is the collision mechanism, which is clearly seen in the example of the Indo-Eurasian interaction. According to the new reconstructions [*Yang, 2013*], starting from 100 million years ago in the East Asia, there was a frontal collision and oblique interaction between the North China block and the Okhotsk block of Izanagi plate. With this interaction, the author associates intense intra-continental compressional deformations within East China, which occurred right up to the end of the Cretaceous. Thirdly, the back-arc spreading in the marginal seas of the Pacific subduction zone commenced 65 Ma ago, and later on, about 15 Ma ago (Middle Miocene), spreading was replaced by compression [*Yin, 2010*]. This is evidenced by the cessation of the back-arc spreading in the Japan and South China seas, the development of thrust and fold belts in the sediments of the East China and South China seas, and the subduction of the South China basin underneath the Philippine plate. Another evidence is the replacement of transtension with transpression in the Okhotsk Sea and the Sakhalin-Hokkaido fault zone in the Late Miocene [*Worrall et al., 1996*]. Thus, intercontinental deformation in East Asia might have been influenced by the change from extension to compression-transpression in the West Pacific interplate boundary in the Middle Miocene. In particular, this change could caused the redistribution of deformation in the NE periphery of the Indo-Asian collision zone and the cessation of displacements along the Alxa-East Gobi left-lateral strike-slip fault branch 13–16 Ma ago. The NE-striking thrusts may have occurred due to compression. In this case, however, an evidence of similar deformation needs to be discovered not only in the East Gobi depression. Besides, such compression in the Middle Miocene would have acted against the activity of the NE-trending structures in the Dariganga plateau.

Thus, the East Gobi depression is characterized by active deformation in the first half or in the middle of the Cenozoic due to compression. Three potential sources with slightly different directions of compression are the Indo-Asian collision (N-S compression in the Oligocene – Early Miocene), the collision of the North China block of Eurasia and the Okhotsk Sea block of Izanagi plate (the beginning of the Paleocene, NW compression) and the Pacific subduction zone (Middle Miocene, NW compression). This region was low active in the Late Cenozoic, although we revealed some indicators of activity, such as the networks of erosional gullies on the low-amplitude uplifts. This is explainable by the fact that the tectonic deformation caused by the interplate interactions due to the Indo-Asian collision was mainly concentrated in the Gobi Altai and the Periordoss rift system, i.e. resulted in the development of the large structures. Besides, the seismic records from this region show low seismic activity [*Dugarmaa, Shlupp, 2000*]. The regional earthquake focal mechanisms show strike-slip and thrust displacements in the earthquake foci with the NE and ENE-trending axes of maximum compression (see Fig. 3) [*San'kov et al., 2011; Radziminovich et al., 2016*]. Thus, the modern state of crustal stresses and the reconstructed paleostress state are characterized by completely different directions of the axis of maximum compression (see Fig. 3). The main faults in the East Gobi depression have the NE strike parallel to the direction of the axis of maximum horizontal compression in the modern stress field, which does not presuppose their high activity under compression.

The South Gobi depression was also in tectonic quiescence in the Late Cretaceous – Paleogene, but its activity (in contrast to the East Gobi depression) commenced in the Late Cenozoic (Late Miocene – Early Pliocene). From the Late Cenozoic, young uplifts and forebergs, that 'cut' the sediments of the Mesozoic basins, develop in this seismically active region (e.g. [*Cunningham, 2007, 2010, 2013; Yanshin, 1975; Bayasgalan et al., 1999*]). In the eastern termination of the Gobi Altai, we

revealed clear indicators of the Pliocene-Quaternary activity of the W-E and NW-striking strike-slip and thrust faults. The stress field reconstructions show compression, transpression and strike-slip regimes with the dominant NE-trending axis of compression (see Fig. 20). The regional earthquake focal mechanisms in the eastern termination of the Gobi Altai show strike-slip and reverse displacements with the NE-trending axis of maximum compression (see Fig. 3) [*San'kov et al., 2011; Radziminovich et al., 2016*]. The modern state of crustal stress correlates with the reconstructed Late Cenozoic paleostress state in both the type and direction of the axis of maximum compression (see Fig. 3). The source of deformation in the Eastern Gobi Altai, as well as in Western and Southwestern Mongolia, is the Indo-Eurasia collision.

6. Conclusion

Having consolidated and compared the field data with the earthquake focal mechanisms in Southeastern Mongolia, we identify two major deformation stages for the study area in the Cenozoic. In the East Gobi depression, the Early Cretaceous NE-trending faults were activated in the Early Cenozoic (most probably, Paleogene) due to the N-S and NW-trending compression, and the thrusts and left-lateral strike-slips were formed. The most probable source of compression was the West Pacific zone of plate interaction. The impact of the Indo-Eurasia collision, however, cannot be excluded. With time, the activity of the NE-striking faults was considerably reduced.

In the South Gobi depression, the structures in the eastern termination of the Gobi Altai were formed in the Pliocene –Quaternary due to the NE-trending compression caused by to the Indo-Eurasia collision. The W-E and WNW-striking left-lateral strike-slip faults and thrusts occurred in this region. These faults remain active at the present stage of the regional geological development.

7. Acknowledgements

Authors thank to Laura Webb and Damien Delvaux who carefully reviewed the manuscript and made numerous helpful suggestions for its improvement. The reported study was supported by RFBR (research project № 17-05-00826_a).

8. References

Badarch G., Cunningham W.D., Windley B.F., 2002. A new terrane subdivision for Mongolia: implications for the Phanerozoic crustal growth of Central Asia. *Journal of Asian Earth Sciences* 21 (1), 87–110. https://doi.org/10.1016/S1367-9120(02)00017-2.

Baljinnyam I., Bayasgalan A., Borisov B.A., Cisternas A., Dem'yanovich M.G., Ganbataar L., Kochetkov V.M., Kurushin R.A., Molnar P., Hervé P., Vashchilov Yu.Ya., 1993. Ruptures of major earthquakes and active deformation in Mongolia and its surroundings. Geological Society of America Memoirs, vol. 181, 62 p. https://doi.org/10.1130/MEM181.

Bayasgalan A., Jackson J., Ritz J.-F., Carretier S., 1999. 'Forebergs', flowers structures, and the development of large intra-continental strike-slip fault: the Gurvan Bogd fault system in Mongolia. *Journal of Structural Geology* 21 (10), 1285–1302. https://doi.org/10.1016/S0191-8141(99)00064-4.

Bird P., 2003. An updated digital model of plate boundaries. *Geochemistry, Geophysics, Geosystems* 4 (3), 1027. https://doi.org/10.1029/2001GC000252.

Carroll A.R., Graham S.A., Smithz M.E., 2010. Walled sedimentary basins of China. *Basin Research* 22 (1), 17–32. https://doi.org/10.1111/j.1365-2117.2009.00458.x.

Constenius K., Coogan J., Erdenebat B., Tully J., Johnson C., Graham S., Cunningham D., 2013. Late Jurassic – Early Cretaceous rifting in the Tugrug and Taatsiin Tsagaan Nuur Basins, Gobi-Altai Region of SW Mongolia – implications for petroleum exploration. In: AAPG Annual Convention and Exhibition, Search and Discovery Article #10485.

Cunningham D., 2007. Structural and topographic characteristics of restraining bend mountain ranges of the Altai, Gobi Altai and easternmost Tien Shan. In: W.D. Cunningham, P. Mann (Eds.), Tectonics of strike-slip restraining and releasing bends. Geological Society, London, Special Publications, vol. 290, p. 219–237. https://doi.org/10.1144/SP290.7.

Cunningham D., 2010. Tectonic setting and structural evolution of the Late Cenozoic Gobi Altai orogeny. In: T.M. Kusky, M.G. Zhai, W.J. Xiao (Eds.), The evolving continents: understanding processes of continental growth and stabilization. Geological Society, London, Special Publication, vol. 338, p. 361–387. https://doi.org/10.1144/SP338.17.

Cunningham D., 2013. Mountain building processes in intracontinental oblique deformation belts: lessons from the Gobi Corridor, Central Asia. *Journal of Structural Geology* 46, 255–282. https://doi.org/10.1016/j.jsg.2012.08.010.

Cunningham D., Davies S., McLean D., 2009. Exhumation of a Cretaceous rift complex within a Late Cenozoic restraining bend, southern Mongolia: implications for the crustal evolution of the Gobi Altai region. *Journal of the Geological Society* 166 (2), 321–333. https://doi.org/10.1144/0016-76492008-082.

Daoudene Y., Gapais D., Ledru P., Cocherie A., Hocquet S., Donskaya T.V., 2009. The Ereendavaa Range (north-eastern Mongolia): an additional argument for Mesozoic extension throughout eastern Asia. *International Journal of Earth Sciences* 98 (6), 1381–1393. https://doi.org/10.1007/s00531-008-0412-2.

Darby B.J., Ritts B.D., Yue Y., Meng Q., 2005. Did the Altyn Tagh fault extend beyond the Tibetan Plateau? *Earth and Planetary Science Letters* 240 (2), 425–435. https://doi.org/10.1016/j.epsl.2005.09.011.

Davis G.A., Darby B.J., Yadong Z., Spell T.L., 2002. Geometric and temporal evolution of an extensional detachment fault, Hohhot metamorphic core complex, Inner Mongolia, China. *Geology* 30 (11), 1003–1006. https://doi.org/10.1130/0091-7613(2002)030%3C1003:GATEOA%3E2.0.CO;2.

Davis G.A., Qian X., Zheng Y.D., Tong H.M., Yu H., Gehrels G., Shafiqullah M., Fryxell J., 1996. Mesozoic deformation and plutonism in the Yunmeng Shan: a metamorphic core complex north of Beijing, China. In: A. Yin, T.M. Harrison (Eds.), The tectonic evolution of Asia. Cambridge University Press, Cambridge, p. 253–280.

Delvaux D., 1993. The TENSOR programm for reconstruction: examples from east African and the Baikal rift systems. *Terra Abstracts. Abstract Supplement to Terra Nova* 5, 216.

Delvaux D., 2012. Release of program Win-Tensor 4.0 for tectonic stress inversion: statistical expression of stress parameters. *Geophysical Research Abstracts* 14, EGU2012-5899. Available from: https://meetingorganizer.copernicus.org/EGU2012/EGU2012-5899.pdf (Software available from: http://users.skynet.be/damien.delvaux/Tensor/tensor-index.html).

Delvaux D., Moeys R., Stapel G., Petit C., Levi K., Miroshnichenko A., Ruzhich V., Sankov V., 1997. Paleostress reconstructions and geodynamics of the Baikal region, Central Asia, Part 2. Cenozoic rifting. *Tectonophysics* 282 (1–4), 1–38. https://doi.org/10.1016/S0040-1951(97)00210-2.

Delvaux D., Moyes R., Stapel G., Melnikov A., Ermikov V., 1995. Paleostress reconstruction and geodynamics of the Baikal region, Central Asia, Part 1. Palaeozoic and Mesozoic pre-rift evolution. *Tectonophysics* 252 (1–4), 61–101. https://doi.org/10.1016/0040-1951(95)00090-9.

Dill H.G., Altangerel S., Bulgamaa J., Hongor O., Khishigsuren S., Majigsuren Yo., Myagmarsuren S., Heunisch C., 2004. The Baganuur coal deposit, Mongolia: depositional environments and paleoecology of a Lower Cretaceous coal-bearing intermontane basin in Eastern Asia. *International Journal of Coal Geology* 60 (2–4), 197–236. https://doi.org/10.1016/j.coal.2003.09.008.

Dugarmaa T., Shlupp A. (Eds.), 2000. One Century of Seismicity of Mongolia. CAG MAS, Ulaanbaatar, 141 p.

Feng Z.Q., Jia C.Z., Xie X.N., Zhang S., Feng Z.H., Cross A.T., 2010. Tectonostratigraphic units and stratigraphic sequences of the nonmarine Songliao basin, northeast China. *Basin Research* 22 (1), 79–95. https://doi.org/10.1111/j.1365-2117.2009.00445.x.

Florensov N.A., Solonenko V.P., 1963. The Gobi-Altai Earthquake. Publishing House of the USSR Acad. Sci., Moscow, 391 p. (in Russian) [Гоби-Алтайское землетрясение / Ред. Н.А. Флоренсов, В.П. Солоненко. М.: Изд-во АН СССР, 1963. 391 с.].

Graham S.A., Hendrix M.S., Johnson C.L., Badamgarav D., Badarch G., Amory J., Porter M., Barsbold R., Webb L.E., Hacker B.R., 2001. Sedimentary record and tectonic implications of Mesozoic rifting in southeast Mongolia. *Geological Society of America Bulletin* 113 (12), 1560–1579. https://doi.org/10.1130/0016-7606(2001)113%3C1560:SRATIO%3E2.0.CO;2.

Horton B.K., Constenius K.N., Tully J., Coogan J.C., Menotti T., Buyan-Arivjikh D., Yasli M., Erdenejav U., Payton A., 2013. Late Jurassic – Early Cretaceous Synrift Sedimentation in the Tsagaan Suvarga Basin, Gobi-Altai Region of SW Mongolia. In: AAPG Annual Convention and Exhibition, Search and Discovery Article #10487.

Howard J.P., Cunningham W.D., Davies S.J., 2006. Competing processes of clastic deposition and compartmentalized inversion in an actively evolving transpressional basin, Western Mongolia. *Journal of the Geological Society* 163 (4), 657–670. https://doi.org/10.1144/0016-764904-073.

Howard J.P., Cunningham W.D., Davies S.J., Dijkstra A.H., Badarch G., 2003. The stratigraphic and structural evolution of the Dzereg Basin, Western Mongolia: clastic sedimentation, transpressional faulting and basin destruction in an intraplate, intracontinental setting. *Basin Research* 15 (1), 45–72. https://doi.org/10.1046/j.1365-2117.2003.00198.x.

Johnson C.L., 2004. Polyphase evolution of the East Gobi basin: sedimentary and structural records of Mesozoic-Cenozoic intraplate deformation in Mongolia. *Basin Research* 16 (1), 79–99. https://doi.org/10.1111/j.1365-2117.2004.00221.x.

Johnson L., Constenius K., Graham S., Mackey G., Menotti T., Payton A., Tully J., 2015. Subsurface evidence for Late Mesozoic extension in Western Mongolia: tectonic and petroleum systems implications. *Basin Research* 27 (3), 272–294. https://doi.org/10.1111/bre.12073.

Leonov M.G., 2012. Within-plate zones of concentrated deformation: Tectonic structure and evolution. *Geotectonics* 46 (6), 389–411. https://doi.org/10.1134/S0016852112060052.

Levi K.G., 2007. New neotectonic map of the northeastern sector of Asia. In: Geodynamic evolution of the lithosphere of the Central Asian mobile belt (from ocean to continent). Issue 5, Vol. 1. Institute of the Earth's Crust of SB RAS, Irkutsk, p. 136–139 (in Russian) [*Леви К.Г.* Новая неотектоническая карта северо-восточного сектора Азии // Геодинамическая эволюция литосферы Центрально-Азиатского подвижного пояса (от океана к континенту). Вып. 5. Иркутск: ИЗК СО РАН, 2007. Т. 1. С. 136–139].

Li K., Jolivet M., Zhang Z., Li J., Tang W., 2016. Long-term exhumation history of the Inner Mongolian Plateau constrained by apatite fission track analysis. *Tectonophysics* 666, 121–133. https://doi.org/10.1016/j.tecto.2015.10.020.

Marinov N.A., Zonenshain L.P., Blagonravov V.A. (Eds.), 1973. Geology of the Mongolian People's Republic. Vol. 1. Stratigraphy. Nedra, Moscow, 584 p. (in Russian) [Геология Монгольской Народной Республики. Том 1. Стратиграфия / Ред. Н.А. Маринов, Л.П. Зоненшайн, В.А. Благонравов. М.: Недра, 1973. 584 с.].

Mazukabzov A.M., Donskaya T.V., Gladkochub D.P., Sklyarov E.V.,Ponomarchuk V.A., Sal'nikova E.B., 2006. Structure and age of the metamorphic core complex of the Burgutui ridge (Southwestern Transbaikal region). *Doklady Earth Sciences* 407 (2), 179–183. https://doi.org/10.1134/S1028334X06020048.

Mazukabzov A.M., Gladkochub D.P., Donskaya T.V., Sklyarov E.V., Ripp G.S., Izbrodin I.A., Wang T., Zeng L.S., 2011. The Selenga metamorphic core complex (Western Transbaikalian Region). *Doklady Earth Sciences* 440 (1), 1212–1215. https://doi.org/10.1134/S1028334X11090066.

Meng Q.-R., 2003. What drove late Mesozoic extension of the northern China–Mongolia tract? *Tectonophysics* 369 (3–4), 155–174. https://doi.org/10.1016/S0040-1951(03)00195-1.

Metelkin D.V., Gordienko I.V., Klimuk V.S., 2007. Paleomagnetism of Upper Jurassic basalts from Transbaikalia: new data on the time of closure of the Mongol-Okhotsk Ocean and Mesozoic intraplate tectonics of Central Asia. *Russian Geology and Geophysics* 48 (10), 825–834. https://doi.org/10.1016/j.rgg.2007.09.004.

Radziminovich N.A., Bayar G., Miroshnichenko A.I., Demberel S., Ulzibat M., Ganzorig D., Lukhnev A.V., 2016. Focal mechanisms of earthquakes and stress field of the crust in Mongolia and its surroundings. *Geodynamics and Tectonophysics* 7 (1), 23–38. https://doi.org/10.5800/GT-2016-7-1-0195.

Ritts B.D., Berry A.K., Johnson C.L., Darby B.J., Davis G.A., 2010. Early Cretaceous supradetachment basins in the Hohhot metamorphic core complex, Inner Mongolia, China. *Basin Research* 22 (1), 45–60. https://doi.org/10.1111/j.1365-2117.2009.00433.x.

San'kov V.A., Parfeevets A.V., Lukhnev A.V., Miroshnichenko A.I., Ashurkov S.V., 2011. Late Cenozoic geodynamics and mechanical coupling of crustal and upper mantle deformations in the Mongolia-Siberia mobile area. *Geotectonics* 45 (5), 378–393. https://doi.org/10.1134/S0016852111050049.

Sherman S.I., Kuchay O.A., Bushenkova N.A., 2017. Geodynamic and seismic zonation of the formation of the strongest earthquakes in Central Asia. *Interexpo Geo-Siberia* 2 (4), 71–75 (in Russian) [*Шерман С.И., Кучай О.А., Бушенкова Н.А.* Геодинамическая и сейсмическая зональность формирования сильнейших землетрясений Центральной Азии // *Интерэкспо Гео-Сибирь*. 2017. Т. 2. № 4. С. 71–75].

Sherman S.I., Ma Jin, Gorbunova E.A., 2015. Recent strong earthquakes in Central Asia: regular tectonophysical features of locations in the structure and geodynamics of the lithosphere. Part 1. Main geodynamic factors predetermining locations of strong earthquakes in the structure of the lithosphere in Central Asia. Geodynamics & Tectonophysics 6 (4), 409–436. https://doi.org/10.5800/GT-2015-6-4-0188.

Sklyarov E.V., Mazukabzov A.M., Mel'nikov A.I., 1997. Metamorphic Core Complexes of the Cordilleran Type. SPC UIGGM SB RAS, Novosibirsk, 192 p. (in Russian) [*Скляров Е.В., Мазукабзов А.М., Мельников А.И.* Комплексы метаморфических ядер кордильерского типа. Новосибирск: Изд-во РИНЦ ОИГГМ СО РАН, 1997. 192 с.].

Tomurtogoo O. (Ed.), 1999. Geological Map of Mongolia. Scale 1:1000000. Institute of Geology and Mineral Resources, Mongolian Academy of Sciences.

Traynor J.J., Sladen C., 1995. Tectonic and stratigraphic evolution of the Mongolian People's Republic and its influence on hydrocarbon geology and potential. *Marine and Petroleum Geology* 12 (1), 35–52. https://doi.org/10.1016/0264-8172(95)90386-X.

Van der Beek P.A., Delvaux D., Andriessen P.A.M., Levi K.G., 1996. Early Cretaceous denudation related to convergent tectonics in the Baikal region, SE Siberia. *Journal of the Geological Society* 153 (4), 515–523. https://doi.org/10.1144/gsjgs.153.4.0515.

Vincent S.J., Allen M.B., 1999. Evolution of the Minle and Chaoshui Basins, China: Implications for Mesozoic strike-slip basin formation in Central Asia. *Geological Society of America Bulletin* 111 (5), 725–742. https://doi.org/10.1130/0016-7606(1999)111%3C0725:EOTMAC%3E2.3.CO;2.

Wang T., Guo L., Zheng Y., Donskaya T., Gladkochub D., Zeng L., Li J., Wang Y., Mazukabzov A., 2012. Timing and processes of late Mesozoic mid-lower-crustal extension in continental NE Asia and implications for the tectonic setting of the destruction of the North China Craton: mainly constrained by zircon U–Pb ages from metamorphic core complexes. *Lithos* 154, 315–345. https://doi.org/10.1016/j.lithos.2012.07.020.

Watson M.P., Hayward A.B., Parkinson D.N., Zhang Z.M., 1987. Plate tectonic history, basin development and petroleum source rock deposition onshore China. *Marine and Petroleum Geology* 4 (3), 205–225. https://doi.org/10.1016/0264-8172(87)90045-6.

Webb L.E., Graham S.A., Johnson C.L., Badarch G., Hendrix M.S., 1999. Occurrence, age, and implications of the Yagan–Onch Hayrhan metamorphic core complex, southern Mongolia. *Geology* 27 (2), 143–146. https://doi.org/10.1130/0091-7613(1999)027%3C0143:OAAIOT%3E2.3.CO;2.

Webb L.E., Johnson C.L., 2006. Tertiary strike-slip faulting in southeastern Mongolia and implications for Asian tectonics. *Earth and Planetary Science Letters* 241 (1–2), 323–335. https://doi.org/10.1016/j.epsl.2005.10.033.

Worrall D.M., Kruglyak V., Kunst F., Kuznetsov V., 1996. Tertiary tectonics of the Sea of Okhotsk, Russia: Far-field effects of the India-Eurasia collision. *Tectonics* 15 (4), 813–826. https://doi.org/10.1029/95TC03684.

Yang Y.T., 2013. An unrecognized major collision of the Okhotomorsk block with East Asia during the Late Cretaceous, constraints on the plate reorganization of the Northwest Pacific. *Earth-Science Reviews* 126, 96–115. https://doi.org/10.1016/j.earscirev.2013.07.010.

Yanshin A.L. (Ed.), 1975. Mesozoic and Cenozoic Tectonics and Magmatism of Mongolia (Proceedings of the Joint Soviet-Mongolian Geological Expedition, Issue 11). Nauka, Moscow, 308 p. (in Russian) [Мезозойская и кайнозойская тектоника и магматизм Монголии / Ред. А.Л. Яншин (Труды совместной советско-монгольской геологической экспедиции, вып. 11). М.: Наука, 1975. 308 с.].

Yin A., 2010. Cenozoic tectonic evolution of Asia: A preliminary synthesis. *Tectonophysics* 488 (1–4), 293–325. https://doi.org/10.1016/j.tecto.2009.06.002.

Yue Y., Liou J.G., 1999. Two-stage evolution model for the Altyn Tagh fault, China. *Geology* 27 (3), 227–230. https://doi.org/10.1130/0091-7613(1999)027%3C0227:TSEMFT%3E2.3.CO;2.

Zhang F., Wu Z., Li W., 2018. Structural anatomy and dynamics of evolution of the Huanghua Depression during the Indosinian-Yanshan movement: Implication for the destruction of North China Craton. *Geophysical Research Abstracts* 20, EGU2018-7072. Available from: https://meetingorganizer.copernicus.org/EGU2018/EGU2018-7072.pdf.

Zonenshain L.P., Savostin L.A., 1979. Introduction to Geodynamics. Nedra, Moscow, 234 pp. (in Russian) [*Зоненшайн Л.П., Савостин Л.А.* Введение в геодинамику. М.: Недра, 1979. 311 с.].

Zorin Y.A., 1999. Geodynamics of the western part of the Mongolia–Okhotsk collisional belt, Trans-Baikal region (Russia) and Mongolia. *Tectonophysics* 306 (1), 33–56. https://doi.org/10.1016/S0040-1951(99)00042-6.

Anna V. Parfeevets, Candidate of Geology and Mineralogy, Researcher
Institute of the Earth's Crust, Siberian Branch of RAS
128 Lermontov street, Irkutsk 664033, Russia

✉ e-mail: aparf@crust.irk.ru
ORCID ID https://orcid.org/0000-0003-1526-1329

Анна Владимировна Парфеевец, канд. геол.-мин. наук, н.с.
Институт земной коры СО РАН
664033, Иркутск, ул. Лермонтова, 128, Россия

Vladimir A. Sankov, Candidate of Geology and Mineralogy, Head of Laboratory
Institute of the Earth's Crust, Siberian Branch of RAS
128 Lermontov street, Irkutsk 664033, Russia
Irkutsk State University, Geological Faculty
3 Lenin street, Irkutsk 664003, Russia

e-mail: sankov@crust.irk.ru
ORCID ID https://orcid.org/0000-0002-1066-2601

Владимир Анатольевич Саньков, канд. геол.-мин. наук, зав. лабораторией
Институт земной коры СО РАН
664033, Иркутск, ул. Лермонтова, 128, Россия
Иркутский государственный университет, геологический факультет
664003, Иркутск, ул. Ленина, 3, Россия
e-mail: sankov@crust.irk.ru